

NASA TECHNICAL NOTE



NASA TN D-8185

NASA TN D-8185



LOAN COPY: RETURN TO
AFWL TECHNICAL LIBRARY
KIRTLAND AFB, N. M.

MECHANICAL CAPACITOR

*James A. Kirk, Philip A. Studer,
and Harold E. Evans*


*Goddard Space Flight Center
Greenbelt, Md. 20771*





0133840

1. Report No. NASA TN D-8185		2. Government Accession No.		3. Recipient's Catalog No.	
4. Title and Subtitle Mechanical Capacitor				5. Report Date March 1976	
7. Author(s) James A. Kirk, Philip A. Studer, and Harold E. Evans				6. Performing Organization Code 721	
9. Performing Organization Name and Address Goddard Space Flight Center Greenbelt, Maryland 20771				8. Performing Organization Report No. G-7639	
12. Sponsoring Agency Name and Address National Aeronautics and Space Administration Washington, D. C. 20546				10. Work Unit No. 778-52-01-01	
15. Supplementary Notes				11. Contract or Grant No.	
16. Abstract A new energy storage system (the mechanical capacitor), using a spokeless magnetically levitated composite ring rotor, is described, and design formulas for sizing the components are presented. This new system is configured around a permanent magnet (flux biased) suspension which has active servo control in the radial direction and passive control in the axial direction. The storage ring is used as a moving rotor and electronic commutation of the stationary armature coils is proposed. There is no mechanical contact with the rotating spokeless ring, therefore, long life and near zero rundown losses are projected. A 7-kW h system is sized to demonstrate feasibility. Also, literature review of flywheel energy storage systems is presented and general formulas are developed for comparing rotor geometries.				13. Type of Report and Period Covered Technical Note	
17. Key Words (Selected by Author(s)) Energy storage, Solar energy, Wind energy, Emergency power, Flywheel energy				14. Sponsoring Agency Code	
				18. Distribution Statement Unclassified--Unlimited Cat. 44	
19. Security Classif. (of this report) Unclassified	20. Security Classif. (of this page) Unclassified	21. No. of Pages 56	22. Price* \$4.25		



This document makes use of international metric units according to the Systeme International d'Unites (SI). In certain cases, utility requires the retention of other systems of units in addition to the SI units. The conventional units stated in parentheses following the computed SI equivalents are the basis of the measurements and calculations reported.

SYMBOLS

<u>Symbol</u>	<u>Name</u>	<u>Units</u>
K. E.	Kinetic energy	J
E_w	Kinetic energy per unit of rotor weight, termed energy density	J/N
σ_{max}	Maximum centrifugal stress	Pa
σ_r	Radial centrifugal stress	Pa
σ_θ	Circumferential centrifugal stress	Pa
K_s	Flywheel rotor shape factor	—
E_{vs}	Kinetic energy per unit of swept rotor volume	Pa
W/V_s	Rotor weight per unit of rotor swept volume	N/m^3
τ	Thickness of rotor or of a square single filament	m
R	Radial thickness of a round single filament	m
γ	Weight density of material	N/m^3
a	Inner rotor radius	m
b	Outer rotor radius	m
ν	Poisson ratio of contraction in the radial direction due to extension in the circumferential direction	—
ID	Inside diameter	m
OD	Outside diameter	m
ω	Angular velocity	rad/s
N	Rotations per minute	rot/min

<u>Symbol</u>	<u>Name</u>	<u>Units</u>
$W(\omega)$	Parasitic losses in an energy storage system— a function of angular rotor speed	W
$P(\omega)$	Load or input power for an energy storage system— a function of angular rotor speed	W
$\zeta(\omega)$	Efficiency of power transfer in an energy storage system—a function of angular rotor speed	-
J_g	Flywheel polar moment of inertia	J_s^2
W_t	Total load on an energy storage system $W(\omega) + P(\omega)$	W
n	The number of single filaments in a “brush” superflywheel	-
$P(\text{laminar})$	Windage losses assuming laminar fluid flow	W
$P(\text{molecularflow})$	Windage losses assuming molecular stream fluid flow	W
r	Radius from center of rotation	m
Wh	Watt hours	Wh
lbf	Pounds force	lbf

CONTENTS

	<i>Page</i>
ABSTRACT	i
SYMBOLS	iii
INTRODUCTION	1
THE GENERAL ENERGY STORAGE SYSTEM	5
FLYWHEEL ROTORS	7
THE RING FLYWHEEL STORAGE SYSTEM	14
DISCUSSION OF THE RING STORAGE MODULES	16
CONCLUSIONS	25
SUGGESTIONS FOR FUTURE WORK	26
REFERENCES	27
APPENDIX A—SUMMARY OF UNIT CONVERSIONS	29
APPENDIX B—EVALUATION OF VARIOUS ROTOR SHAPES	31
APPENDIX C—ID/OD RATIO TO ELIMINATE RADIAL DELAMINATION DUE TO CENTRIFUGAL STRESSES	37
APPENDIX D—SIMPLIFIED DESIGN EQUATIONS FOR SIZING A STORAGE ROTOR	41
APPENDIX E—WINDAGE LOSSES FOR A RING FLYWHEEL	45
APPENDIX F—FLYWHEEL—SUSPENSION	49
APPENDIX G—MOTOR/GENERATOR CALCULATIONS	51

MECHANICAL CAPACITOR

James A. Kirk

*University of Maryland
College Park, Maryland*

**Philip A. Studer and
Harold E. Evans**

*Goddard Space Flight Center
Greenbelt, Maryland*

INTRODUCTION

One of the main purposes of energy storage is to conserve petroleum resources through the reduction in both the dollar and the environmental costs of providing energy to the consumer. The basic problem facing utility companies is, and will continue to be, variations in the demand for electric power. Kalhammer and Zygielbaum (reference 1), Keller (reference 2), and Rabenhorst* point out that electric utilities use:

- Base load generators to serve the load which continues 24 hours a day. This function is served by the more efficient fossil fuel or nuclear generators which operate nearly 100 percent of the time at full throttle. Typically, the base load is approximately 45 percent of the peak load and 70 percent of the system power output.
- Intermediate load generators serve the broad daily demand peak. This function is served with older, less efficient fossil fuel steam generators and gas turbines; these are normally shut down at night.
- Peak load generators serve the immediate load peaks of the day. These are typically gas turbines or diesel engines.

As Keller points out, the base load generators may supply about 70 percent of the total systems power at the lowest delivered cost, while the intermediate load generators will furnish about 25 percent of the power at significantly higher cost. The remaining power is derived from peak load generators which, although relatively inexpensive in terms of capital investment, require costly and scarce special fuels (such as number 2 fuel oil), operate at low efficiencies, and necessitate high expenditures for maintenance.

*Rabenhorst, D.W., "Use of Flywheels for Energy Storage," presented at American Chemical Society, Fall 1974 Meeting of Energy Storage Symposium, Atlantic City, New Jersey, September 12, 1974.

With the cost of fuel increasing rapidly, it is extremely expensive to run the intermediate and peak load generators. Laaspere and Converse (reference 3), for example, point out that the Central Vermont Public Service Corporation has introduced a rate option where electricity used between 8 and 11 a.m. and between 5 and 9 p.m. costs six times more than that used at other times. This type of costing differential provides the economic impetus for the development and installation of high efficiency energy storage systems.

In the past, electric utilities have attempted to reduce the high cost of peak power generation through pumped hydroelectric storage (reference 4). Typically, water is pumped up hill during off peak hours and stored in a reservoir for later peak hour use. This method is approximately 66 percent efficient (reference 4) and is limited to those locations where geography permits the construction of large reservoirs. As an example, a 1900-MW, 15,000-MW h system is jointly operated by the Consumers Power Company and Detroit Edison Company. The storage reservoir is a manmade lake more than 3 by 1.5 km (1.86 by 0.93 mi) constructed at a cost of more than \$300 million. To deliver the required amount of power, roughly 10^8 m³ of water must be pumped and discharged, and the overall system represents a capital cost of approximately \$200/kW. Furthermore, the stored energy density is quite low (reference 2)—81 J/N (0.1 W h/lbf).

There are numerous mechanisms which are theoretically capable of storing energy. The following list describes some of those mechanisms which are currently under consideration for electric utility storage systems:

- Mechanical—flywheels (kinetic energy),
- Mechanical—pumped water storage (potential energy),
- Mechanical—compressed air storage (potential energy),
- Chemical—fuel cells,
- Electrical—secondary storage batteries, and
- Electrical—superconducting magnet.

Not all of these mechanisms are sufficiently technically developed nor economically feasible for application to a complete system of electric utility energy storage.

Kalhammer and Zygielbaum (reference 1) have compared various storage systems which utilize the six mechanisms previously mentioned, and they conclude that flywheel energy storage will be viable in utility application when acceptable reliability and long lifetimes can be assured. They suggest that lifetimes greater than 20 years and power conversion efficiencies greater than 60 percent will be needed to make flywheels applicable to peak shaving for distributed utility energy storage systems.

The concept of energy storage in rotating flywheels is not new; Clerk (reference 5) has provided a useful history of the development of flywheel systems. Clerk points out that the most severe practical limitations of stored kinetic energy systems have been parasitic

losses due to friction, windage, relatively poor energy storage per unit weight of flywheel, and the hazard of catastrophic failure of the rotor.

Before discussing recent work on flywheel energy storage systems it is useful to consider measures of performance which are used to compare maximum storage capabilities among various flywheel configurations. The following quantities have been used by numerous authors throughout the literature.

<u>Symbol</u>	<u>Description</u>	<u>Unit</u>
E_w	Energy density—stored kinetic energy per unit of flywheel weight	J/N (W h/lbf)
E_{vs}	Stored kinetic energy per unit of swept flywheel volume	Pa (psi)
W/V_s	Flywheel weight per unit of flywheel swept volume	N/m ³ (lbf/in. ³)
K_s	Nondimensional factor for comparing the effectiveness of various flywheel shapes—maximum 1.0	—
σ/γ	Flywheel specific strength, maximum working stress in flywheel per unit of weight density	J/N (W h/lbf)

The following equation (discussed in the section on flywheel rotors) governs the energy density for any given flywheel configuration.

$$E_w = K_s \frac{\sigma}{\gamma} \quad (1)$$

Also, the following relationship governs E_w , E_{vs} , and W/V_s .

$$W/V_s = E_{vs}/E_w \quad (2)$$

Useful conversion factors for manipulating many of the energy storage units found in the literature to a common system are shown in appendix A.

Rabenhorst (references 6 through 13) was among the first investigators to show that anisotropic (composite) materials have capabilities of extremely large specific strengths in flywheel applications. For example (reference 6), a 70 percent graphite whisker/epoxy has a usable specific strength of 457 kJ/N (565 W h/lbf), while the material Kevlar-49 (reference 13) has capabilities of 88 kJ/N (109 W h/lbf). These values represent a

substantial improvement over maraging steel at 26 kJ/N (32 W h/lbf) and at least an order of magnitude over the lead-acid storage battery (reference 6) at 6.4 kJ/N (8 W h/lbf). Because of the large values of specific strength for anisotropic materials, those kinetic storage systems which allow optimal use of essentially straight anisotropic materials are termed superflywheels. Rotor geometry for composite materials, however, is limited to those geometries that develop nearly unidirectional centrifugal stresses.

There are two basic rotational configurations which develop essentially uniaxial stress patterns, allowing maximum use of the composite material specific strength. These are:

- The fanned circular brush superflywheel as described by Rabenhorst (references 8 through 10). In this configuration a number of thin anisotropic rods are spinning about their minor axis ($K_s = 0.33$ for this configuration).
- The thin rim or multirim superflywheel, as described by Rabenhorst (reference 11) and Post et al. (reference 14). In this configuration a number of independent thin rings (spinning about a common axis) are essentially in pure circumferential uniaxial stress ($K_s = 0.50$ for this configuration).

If either of these flywheel configurations is used in an energy storage system, there must be rotation about a common shaft and either a connection hub (for the brush) or spokes (for the multirim) are required to connect the rotor to the power shaft. Invariably, the superflywheels must operate in a vacuum environment, forcing the designer of a total storage system to deal with potential problems in such items as seals, bearings, pumpdown equipment, enclosures, and electrical/mechanical converters. The magnetically levitated spokeless ring flywheel system described in this report overcomes a number of these potential problems.

As of this writing no complete anisotropic flywheel storage system has been built and tested, although Dugger et al. (references 15 and 16) have evaluated individual single filaments of composite materials in spin tests. Interestingly however, a small 222-N (50-lbf) magnetically suspended, anisotropic ring for angular momentum spacecraft control is currently under test at Langley Research Center (reference 17). A number of the advanced concepts used in this ring were developed at the Goddard Space Flight Center (references 18 through 20) and the application of these concepts to the levitated ring energy storage systems will be described later.

The purpose of the remainder of this report is to:

- Develop a working equation and set general requirements for the kinetic energy storage system,
- Compare rotor geometries for various flywheel configurations,

- o Discuss the magnetically levitated spokeless ring in terms of the required modules which are necessary if the concept is to be implemented as an energy storage system, and
- To suggest a design for a 7 kW h magnetically levitated spokeless ring system which can be used to demonstrate the system.

THE GENERAL ENERGY STORAGE SYSTEM

A block diagram of a rotational kinetic energy storage system is shown in figure 1. The losses of both the storage system and of the electrical conversion elements, which are constantly present parasitic losses, are shown as watts. In general, these losses are a function of the flywheel angular rotational frequency (ω) and are present during both charge and discharge cycling.

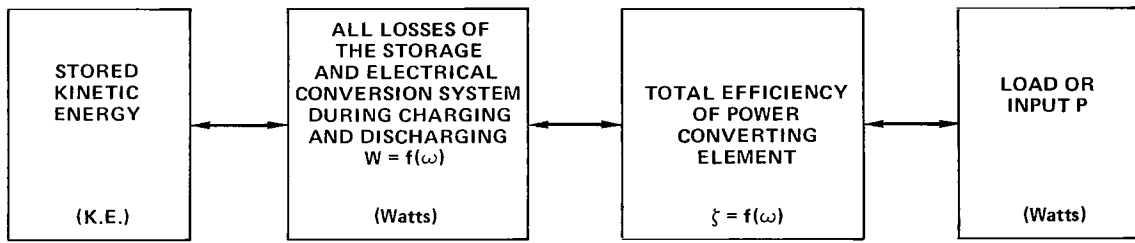


Figure 1. Block diagram of flywheel energy storage system.

As soon as power flow begins (either charge or discharge), the efficiency of the converting elements (which can also be a function of angular rotational frequency) enters the calculation.

If an equation for the energy balance of this system is written, then:

$$\frac{d \text{K.E.}}{dt} = -W(\omega) - P(\omega)/\zeta(\omega) \quad \text{Discharge cycle} \quad (3)$$

$$\frac{d \text{K.E.}}{dt} = -W(\omega) + P(\omega)/\zeta(\omega) \quad \text{Charge cycle} \quad (3a)$$

		<u>Units</u>	
where:	K.E.	= stored kinetic energy	joules
	t	= time	seconds
	W (ω)	= losses, a function of ω	watts

+ P (ω)	= power input (charge), a function of ω	watts
- P (ω)	= load output (discharge), a function of ω	watts
ζ (ω)	= efficiency of power conversion, a function of ω	-
ω	= angular rotational frequency	radians/second

If the moment of inertia of the flywheel is constant, then (3) may be rewritten as:

$$\frac{d\omega}{dt} = \frac{-W(\omega)}{J_g} - \frac{P(\omega)}{J_g \zeta(\omega)} \quad (4)$$

Units

where: ω	= angular rotational frequency	radians/second
J _g	= flywheel polar moment of inertia	joules · second ²

For the simple case where the load and losses are independent of ω, the kinetic energy decreases linearly with time while ω decreases as the square root of time. For this case:

$$t^* = \frac{9.14 \times 10^{-5} J_g}{W_t} (N_i^2 - N_f^2) \quad (5)$$

Units

where: t*	= time to slow to N _f	minutes
N _i	= initial rotational speed	revolutions per minute
N _f	= final rotational speed	revolutions per minute
J _g	= flywheel polar mass moment of inertia	joules · second ²
W _t	= total load	watts

Those variations of W, P, or ζ (as functions of ω) which are not easily expressible mathematically would require numerical solution of equation (4). This procedure would be used to generate ω versus t plots which could then be converted directly to K.E. versus t (since K.E. = ½ J_g ω²) plots and the time for the system to drop to some percentage of the initial kinetic energy could be obtained directly from the plot.

Based in part upon equations (1) and (5), the requirements of a flywheel storage system are:

- Efficient rotor shapes to take full advantage of rotor strengths,
- Low parasitic losses,
- Reliable operation over long lifetimes,
- High efficiencies of power conversion,
- Minimization of damage in the event of rotor failure, and
- Ability to avoid self-destruction in the event of seismic disturbances.

FLYWHEEL ROTORS

The study of flywheel rotor shapes has received the greatest attention of all the components of the flywheel energy storage system. Lawson (reference 21) and Dugger et al. (references 15 and 16) have analyzed the stored kinetic energy in various flywheel shapes (where centrifugal stresses limit performance) and have produced a listing of numerical shape factors (K_s in equation (1)) for particular geometrics. Unfortunately, the numerical shape factors depend on geometrical properties of the specific rotor shape, and general formulas are not provided by either Lawson or Dugger.

The problem of rotor shape characterization is best visualized by referring to figure 2. For any rotor shape, the following information should be expressible in mathematical form in order to evaluate rotor performance:

- K.E. – stored kinetic energy in the rotor,
- E_w – kinetic energy per unit of rotor weight,
- σ_{\max} – the maximum (limiting) allowable centrifugal stress in the rotor,
- K_s – the nondimensional shape factor for a given geometry,
- E_{vs} – kinetic energy per unit of swept volume, and
- W/V_s – rotor weight per unit of swept volume.

For all of the assumed flywheel geometries which are analyzed in this report, the following procedure is used to characterize the rotor:

1. An expression is written for the kinetic energy of the rotor.
2. The kinetic energy expression is divided by the weight of the rotor to form E_w .

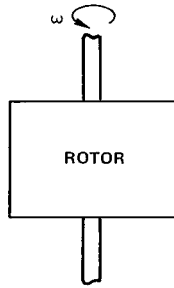


Figure 2. Flywheel rotor characterization.

3. An expression is written for the magnitude of the maximum centrifugal stress, and this is used to eliminate ω from the E_w expression.
4. The expression for E_w is multiplied by the rotor weight and divided by the swept volume to obtain an expression for E_{vs} .
5. The expression for W/V_s is obtained by dividing E_w into E_{vs} .

Applying steps 1 through 3 results in an expression of the form:

$$E_w = K_s \times \frac{\sigma}{\gamma}$$

which has been given previously in equation (1). In this expression, K_s depends only on rotor geometry.

General rotor shape characterization formulas are shown in appendix B for the following geometries:

1. Constant stress disk—A rotor shape selected such that $\sigma_r = \sigma_\theta = \sigma_{\max} = \text{constant}$, everywhere in the rotor (reference 22).
2. Pierced disk (ring)—A constant thickness rotor analyzed for both radial and circumferential stresses (treated as isotropic for this analysis).
3. Hoop—A thin (ID/OD approaches 1.0) constant thickness pierced disk, where it is assumed $\sigma_r = 0$. A given swept volume could be occupied by a number of independent hoops with the effect of the overall ID/OD ratio being much less than 1.0. For this case the hoop formulas would still apply. (This was the multirim analysis used by Rabenhorst (reference 11).)
4. Round single filament—A single round rod rotating about its minor axis.
5. Square single filament—A single square rod rotating about its minor axis.
6. Brush— n single filaments (either round or square) all rotating about a common minor axis and in the same thickness plane (references 8 and 13).

The particular geometrics were selected because of the following reasons:

- They are the only configurations which provide nearly uniaxial centrifugal loading, thus allowing the use of the maximum strength properties of anisotropic materials.
- They have been suggested by both Rabenhorst and Post as “best” rotor geometrics.

A comparison of the general formulas for the above six shapes is shown in table 1.

To compare the shape factors of various rotor geometries, specific inside-to-outside radius a/b must be selected. Based upon Rabenhorst’s discussion of the brush and multirim flywheels (reference 11), two cases are suggested.

1. The a/b ratio where the volume occupied by the rotor divided by the volume swept by the rotor is the same as for the brush flywheel (approximately 15 percent). This requires $a/b = 0.92$.
2. The a/b ratio where the energy density for the hoop is the same as the energy density for the single filament and brush. This requires $a/b = 0.58$.

A comparison of rotor performance for these two cases is shown in table 2. For the square single filament and brush, it has been assumed $n = 20$, $\tau = 1.2$ cm (0.5 in.) and $2b = 2.25$ m (88 in.) after Rabenhorst and Taylor (reference 13).

Table 1
Comparison of Rotors

Shape	E_u	E_v	W/V_s
Constant stress disk ID = 0 OD = ∞ (best case)	$1.000 \times \frac{\sigma}{\gamma}$	$K_s \times \sigma$	γ
Pierced disk	$\frac{\left(\frac{a}{b}\right)^2 + 1}{3 + \nu + \left(\frac{a}{b}\right)^2 (1 - \nu)} \times \frac{\sigma}{\gamma}$	$K_s \times \sigma \left(1 - \left[\frac{a}{b}\right]^2\right)$	$\gamma \times \left(1 - \left[\frac{a}{b}\right]^2\right)$
Hoop	$\frac{\left(\frac{a}{b}\right)^2 + 1}{4} \times \frac{\sigma}{\gamma}$	$K_s \times \sigma \left(1 - \left[\frac{a}{b}\right]^2\right)$	$\gamma \times \left(1 - \left[\frac{a}{b}\right]^2\right)$
Single filament			
Square	$\left(\frac{1}{3} + \frac{1}{12} \left(\frac{r}{b}\right)^2\right) \times \frac{\sigma}{\gamma}$	$K_s \times \sigma \times \frac{2r}{\pi b}$	$\gamma \times \frac{2r}{\pi b}$
Round	$\left(\frac{1}{3} + \frac{1}{4} \left(\frac{R}{b}\right)^2\right) \times \frac{\sigma}{\gamma}$	$K_s \times \sigma \times \left(\frac{R}{b}\right)$	$\gamma \times \left(\frac{R}{b}\right)$
Brush square single filaments	$\frac{1}{3} \times \frac{\sigma}{\gamma}$	$K_s \times \frac{2n\tau}{\pi b}$	$\gamma \times \frac{2n\tau}{\pi b}$

For electric utility storage systems, long life, reliable operation, high efficiency, and low cost are primary requirements. However, only the rotor is being compared in table 2. Furthermore, the comparison does not include fabrication costs or other strength limiting factors (besides centrifugal stresses) which may arise when a rotor is assembled as part of a complete storage system. Bearing in mind these limitations, the following conclusions are drawn:

- Based on E_w , the hoop and pierced disk are better than the brush for inside-to-outside diameter ratios ≥ 0.58 .
- The hoop and pierced disk are nearly identical for both E_w , E_{vs} , and W/V_s . This is expected because the hoop was analyzed as a special case of the pierced disk.
- The constant stress disk is limited to isotropic materials because $\sigma_r = \sigma_\theta = \sigma =$ constant throughout the disk.
- For the pierced disk or hoop to be competitive with a constant stress disk, the composite material must have a usable specific strength (σ/γ) greater than 2.13 (1.00/0.47) of the best isotropic material which is potentially available for a constant stress disk. Actually, this is a worst case condition since, as Lawson (reference 21) points out, the best practical constant stress disk is limited to $K_s = 0.93$.

A material comparison listing taken from various references as indicated is shown in table 3. Assuming that maraging steel is the highest strength isotropic material for a constant stress rotor (reference 21), then several composite materials have improvement factors greater than 2. In particular, Kevlar-49 is a prime candidate for a composite rotor (it is now selling for approximately \$2 to \$2.50/N (\$8 to \$10 /lbf) but the future price may drop to about \$0.50 to \$0.70/N (\$2 to \$3/lbf) (reference 12)).

A study of energy storage rotors for power and attitude control of spacecraft, an Integrated Power/Attitude Control System (IPACS) has been reported by Notti et al. (references 23 and 24) and Keckler and Jacobs (reference 25). The authors considered the use of the three types of composite materials:

1. Kevlar-49 (PDR -49-III)

$$\sigma_{\max} = 1.38 \text{ G Pa (200,000 psi)}$$

$$\gamma = 13.6 \text{ kN/m}^3 \text{ (0.05 lbf/in.}^3\text{)}$$

$$\frac{\sigma}{\gamma} = 102 \text{ kJ/N (126 W h/lbf)}$$

Table 2
Comparison of Rotor Performance

Shape	E_w	E_v	W/V_s
Constant stress disk (O.D. $\rightarrow \infty$)	$1.000 \frac{g}{\gamma}$	1.00σ	1.00γ
Pierced disk (ring) ($\gamma = 0.3$)	$\frac{a}{b} = 0.92; 0.47 \frac{g}{\gamma}^*$	$0.07 \sigma^*$	0.15γ
Hoop (1 or many)	$\frac{a}{b} = 0.58; 0.38 \frac{g}{\gamma}^\dagger$	$0.25 \sigma^\dagger$	0.66γ
	$\frac{a}{b} = 0.001; 0.30 \frac{g}{\gamma}$	0.30σ	1.00γ
	$\frac{a}{b} = 0.92; 0.46 \frac{g}{\gamma}^*$	$0.07 \sigma^*$	0.15γ
	$\frac{a}{b} = 0.58; 0.33 \frac{g}{\gamma}^\dagger$	$0.22 \sigma^\dagger$	0.66γ
Single filament square	$0.33 \frac{g}{\gamma}$	0.002σ	0.007γ
Brush 20 square single filaments	$0.33 \frac{g}{\gamma}$	0.05σ	0.15γ

* $\frac{a}{b} = 0.92$ This corresponds to W/V_s for the pierced disk and hoop = W/V_s for the brush.

† $\frac{a}{b} = 0.58$ This corresponds to E_w for the hoop = E_w for single filament and brush.

2. Graphite Epoxy

$$\sigma = 1.24 \text{ G Pa (180,000 psi)}$$

$$\gamma = 15.7 \text{ kN/m}^3 \text{ (0.058 lbf/in.}^3\text{)}$$

$$\frac{g}{\gamma} = 78.8 \text{ kJ/N (97.4 W h/lbf)}$$

3. Boron Fibers

$$\sigma = 2.41 \text{ G Pa (350,000 psi)}$$

$$\gamma = 25.5 \text{ kN/m}^3 \text{ (0.094 lbf/in.}^3\text{)}$$

$$\frac{g}{\gamma} = 94.7 \text{ kJ/N (117 W h/lbf)}$$

in a variety of geometrical configurations.

A listing of the results of their study is shown in table 4-A. This may be compared to the results shown in table 4-B which were prepared for a ring with ID/OD = 0.9 ($K_s = 0.45$). Note that the specific energy of the ring rotors are greater than all entries in table 4-A.

Table 3
Comparison of Material Properties

Material	Ultimate Tensile Strength (UTS) $N/m^2 \times 10^8$ (lbf/in. ² $\times 10^3$)	Weight Density D $kg/m^3 \times 10^2$ (lbf/in. ³)	Usable Strength $S = UTS \times 72\%$ $N/m^2 \times 10^8$ (lbf/in. ² $\times 10^3$)	S/D $J/N \times 10^5$ (W h/lbf)	Improvement Over Maraging Steel
Music Wire*	41.34 (600)	78.10 (0.283)	43.48 (431)	0.39 (48)	1.5
Boron/Magnesium*	10.82 (157)	24.01 (0.087)	9.30 (135)	0.39 (48)	1.5
Steel/Epoxy*	29.07 (422)	48.71 (0.1765)	21.22 (308)	0.44 (54)	1.7
Future Music Wire*	68.90 (1000)	78.11 (0.283)	49.61 (720)	0.65 (80)	2.5
Beryllium Wire*	17.23 (250)	18.49 (0.067)	12.40 (180)	0.68 (84)	2.6
Future Boron/Magnesium*	24.12 (350)	24.29 (0.088)	17.36 (252)	0.73 (90)	2.8
Boron/Epoxy*	22.03 (320)	20.42 (0.074)	15.85 (230)	0.79 (98)	3.0
HTS Glass/Epoxy*	22.74 (330)	20.53 (0.0744)	16.39 (238)	0.75 (93)	2.9
Present Graphite/Epoxy*	19.50 (283)	16.00 (0.058)	14.12 (205)	0.88(109)	3.4
Future Glass/Epoxy Prestressed*	32.38 (470)	20.42 (0.074)	23.29 (338)	1.16(143)	4.5
Future Graphite Epoxy*	34.45 (500)	16.56 (0.060)	24.80 (360)	1.52(188)	5.8
Theoretical Future*	84.75 (1230)	17.94 (0.065)	60.98 (885)	3.73(461)	14.3
70% Graphite Whisker/Epoxy*	103.35 (1500)	16.56 (0.060)	74.41 (1080)	4.57(565)	17.6
Kevlar-49†	16.54 (240)	13.80 (0.05)	19.92 (173)	0.88(109)	3.4
Maraging Steel‡	28.18 (409)	79.76 (0.289)	20.26 (294)	0.26 (32)	1.0

*See reference 6.

†See reference 13.

‡See reference 21.

Table 4
Comparison of Rotor Shapes and Performance

A. Comparison of Rotor Shapes (Reference 25)		
Design	Material	Specific Energy W h/kg (W h/lb)
Circular brush	Boron	67.75 (30.76)
Orthotropic disk	Graphite	28.24 (12.82)
Tape wound	PDR-49-III	71.10 (32.28)
	Graphite	60.37 (27.41)
Isotropic	Titanium 6A1-4V	47.75 (21.68)
Isotropic	Steel 300M	34.34 (15.59)
B. Ring Rotor Performance with ID/OD = 0.9 ($K_s = 0.45$)		
Ring	Boron	116.08 (52.7)
Ring	Graphite	96.47 (43.8)
Ring	PDP-49-III	124.89 (56.7)

One entry of interest in table 4-A is the orthotropic disk (that is, pierced disk) which has an effective shape factor of only 0.13 (12.82/97.4). The reason this is much lower than the corresponding entry in table 4-B (for the graphite ring) is that the shape of the orthotropic disk is not thin, and the ultimate speed is limited by the radial delaminating centrifugal stress—a problem not encountered for the ID/OD = 0.9 ring. However, the authors feel that a major reason a thin ring was not considered in the IPACS study was because there was no easy way to couple ring motion to a power source without derating the specific energy of the ring. A method to overcome this difficulty is suggested later in this report.

The results of the rotor study may be summarized as follows:

- The stored energy per unit of weight makes a composite rotor ring (that is, pierced disk with $a/b = 0.9$) flywheel attractive as an energy storage device. Its energy density is superior to a brush rotor for all practical ID/OD geometric ratios.
- The principles of magnetic suspension and brushless commutation (references 26 and 27) can be applied to energy storage rings just as they have been to angular momentum control rings in spacecraft (references 17 through 20).
- The feasibility of constructing a composite storage ring has already been successfully demonstrated for a 222-N (50-lbf) rotor (reference 17).

THE RING FLYWHEEL STORAGE SYSTEM

Figure 3 is a block diagram of the major modules of the complete ring storage system. It is suggested that the storage ring be magnetically suspended and enclosed in a toroidal vacuum container with all the suspension and drive electronics completely enclosed—only wires pierce the enclosure.

The storage module would consist of a flywheel ring rotor configuration as shown in figure 4. The ring could be constructed of a high strength composite material (for example, Kevlar-49) and contain the magnetic suspension components on the inner radius. The center of the inner radius will be used for the motor/generator salient poles, which will be attached to the rotor. The ring will carry only iron material, and only the inner radius of the ring will be used for this purpose.

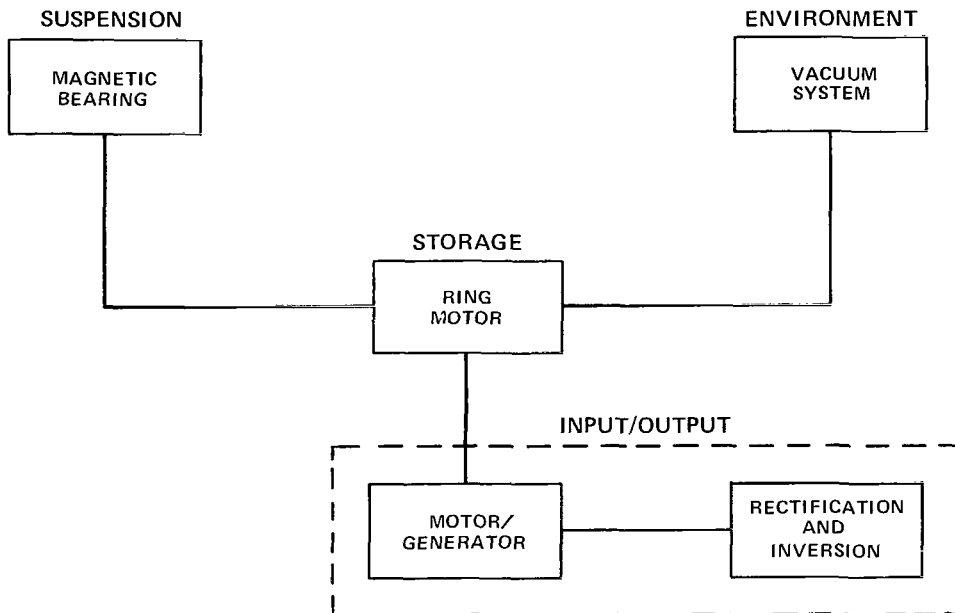


Figure 3. Block diagram of the ring flywheel energy storage modules.

Because the ring is now composed of both a composite material and iron, the overall shape factor will be less than for a single composite material ring. However, the reduction in shape factor may be minimized by proper selection of the magnetic iron material (i.e., trading off some “magnetic softness” for an increase in mechanical strength) or, through an interference fit between the iron and composite ring or, through the use of new high mechanical strength magnetically soft “Metglas” (reference 28).

The environment module would consist of a toroidal enclosure which would house both the rotating ring and the levitation and motor/generator components. This module would consist of vacuum pumpdown equipment which will allow the enclosure to be placed into the 0.13 to 0.0013 Pa (10^{-3} torr to 10^{-5} torr) pressure range. At these pressure levels the parasitic

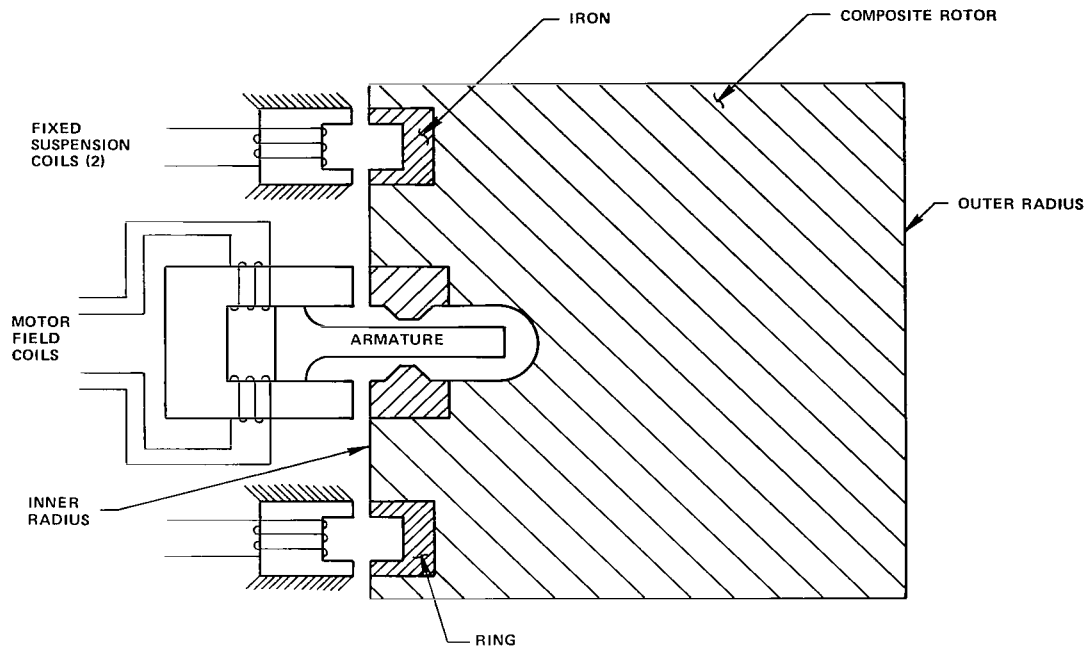


Figure 4. Cross section of the ring rotor.

windage losses will be negligible, and this configuration will not require seals. It is also envisioned that the continuous pumpdown requirements will be minimal since the integrity of the enclosure can be easily maintained.

The suspension module will consist of a circumferential stationary force coil and an iron ring attached to the rotor. The magnetic circuit will establish a magnetic flux across the gap between the moving ring and the stationary coils. Control of rotor position will be passive in the axial direction and active in the radial direction. Because of a unique permanent magnet flux biasing system, the power requirements for radial control will be near zero.*

The motor/generator of the input/output module will consist of a noncontacting, electrically commutated stationary armature which cuts the flux lines of a salient pole variable strength moving field. The electrical output will consist of a periodic voltage (constant amplitude-variable frequency) which will be rectified and then inverted to 60 Hz, 110 V

*Simpson, P.A., "Annular Momentum Control Device (AMCD)–Magnetic Suspension System," Final Report, Subcontract Number 01397, Prime Contract Number NAS1-12529, Cambridge Thermionic Corporation, Cambridge, Massachusetts, 1974.



power. To make the generator function as a motor, 60 Hz 110 V a.c. power will be rectified and fed to the electronic commutation network. This will produce an accelerating torque on the ring which will bring it up to speed.

A comparison of the system requirements for a brush or multirim “conventional” flywheel system and the spokeless levitated ring system are shown in table 5. The primary advantages of the levitated ring concept are:

- Elimination of all conventional bearings (and associated lubrication problems) resulting in increased reliability and long life;
- Elimination of vacuum seals (only electrical wires will penetrate the enclosure system)—also, the need for large continuous pumpdown systems (due to seal leakage) is reduced if not completely eliminated (if outgassing is eliminated a one shot pumpdown will suffice); and
- Elimination of all mechanical contact by the input/output electronically commutated armature resulting in improved reliability and long life. The electrical output will be in the form of alternating voltage and the output from individual, reasonably sized, independent systems can then be combined through a transformer.

DISCUSSION OF THE RING STORAGE MODULES

Storage—The Ring Rotor

The ring rotor (refer to figure 4) contains the energy storage mass (composite ring) along with the “magnetically soft” iron which is required for both the magnetic suspension (suspension module) and the motor/generator (input/output module). The presence of iron will cause an effective reduction in the shape factor of the total ring, but this effect can be minimized (and the overall shape factor caused to approach that of a composite material ring acting alone) by trading off “magnetic softness” with increasing alloy content to improve the mechanical strength of the iron. For purposes of this report, it is assumed that the presence of all iron is negligible (there will be no speed derating due to the iron), and the rotor will be analyzed as if it were simply a constant thickness composite material rotor. If this is true, then the ring rotor must operate under the following strength constraints:

- The speed of the rotor must not cause the maximum circumferential stress to exceed the working stress of the composite material.
- The speed of the rotor must not cause the radial (delaminating) stress to exceed the working cross-fiber strength of the composite material.

Morganthaler and Bonk (reference 29) have shown that the radial and circumferential stress equations for an anisotropic pierced disk approach the classical isotropic formulas (reference 22) as the ID/OD ratio of the disk exceeds 0.9.

Table 5
Comparison of System Requirements for a Conventional versus
Spokeless Levitated Ring Flywheel System

Conventional Flywheel System	Levitated Ring
<p>ROTOR</p> <p>Hub</p> <p>Shaft</p> <p>Storage elements (multirim or brush)</p> <p>Shaft/storage element connection spokes</p>	<p>Single ring storage element (with imbedded iron material)</p>
<p>SUSPENSION</p> <p>Conventional ball bearings</p>	<p>Magnetic levitation (passive axially, active radially)</p>
<p>ENVIRONMENT</p> <p>Vacuum operation</p> <p>Seals required</p> <p>Continuous pumpdown may be required at less than 1.3 N/m² (10⁻² torr)</p> <p>Enclosure system must be larger than OD of flywheel</p>	<p>Vacuum operation (only 1 pumpdown to 0.13 to 0.0013 N/m² (10⁻³ to 10⁻⁵ torr) required)</p> <p>Enclosure system is a toroid with unenclosed center</p>
<p>MOTOR/GENERATOR</p> <p>Synchronous converter required to hold output voltage constant as shaft speed changes</p> <p>Rectifier/inverter required</p>	<p>Synchronous converter not required, special winding provides constant voltage as speed changes</p> <p>Rectifier/inverter required</p>

The flywheel ring may thus be analyzed using the conventional isotropic stress formula provided the above condition is shown to be true. Therefore the following conditions are assumed:

- The classical isotropic σ_r and σ_θ formulas apply to the composite ring rotor.
- The ring will not delaminate as long as the maximum transverse stress (σ_r) is held below 0.5 percent of the maximum fiber stress (σ_θ). According to Post et al. (reference 14), this is a very reasonable assumption.

Thus it can be shown (appendix C) that the ring will not delaminate provided the ID/OD ratio is greater than 0.90).

A greatly simplified design outline for sizing a composite ring rotor is shown in appendix D. It has been included to provide an estimate of rotor size for a 7-kW h system so that typical numbers (for parasitic losses and suspension and motor/generator shares) may be obtained in the sections which follow. The results for a 10-kW h storage ring are summarized in table 6.

Test results by Rabenhorst and by Dugger et al. have shown that when composite fiber rods fail they do so by delamination instead of rapid crack propagation. Typically, only 2 percent of the rotational kinetic energy was actually transported to the rotor container during overspeed failures. This may be contrasted with steel rotor failures which absorb little energy and cause the rotor to break into as few as three large pieces. It is thus anticipated that the containment problems of an overspeed failure for a ring composite rotor would be minimal. Furthermore, the ring system described in this report could easily be placed underground, completely eliminating any hazard to human life in the event of a failure.

Table 6
(7 kW h full to half speed)
Shape and Speed for a 10-kW h Storage Ring made of Kevlar-49 Composite Material

Weight	1085 N (244 lbf)
OD	2.0 m (79 in.)
ID	1.8 m (71 in.)
Thickness	13.4 cm (5.3 in.)
Angular speed	855 rad/s (8163 RPM)
OD tip speed	855 m/s (2805 ft/s)
Mach tip speed	2.54

Environment

The purpose of controlling the ring environment is to minimize windage losses of the spinning rotor. As the tip speed of the rotor increases and the enclosure pressure decreases, the fluid begins to look increasingly like a molecular stream, and the conventional drag coefficients (based only on the Reynolds number) no longer apply. Rohsenow and Choi (reference 30) provide drag coefficient formulas for the molecular stream region, and these have been incorporated into the windage loss equations which are derived in appendix E.

A summary of the total windage losses for the rotor described in table 6 is shown in table 7. The losses P (laminar) are those which are calculated by assuming that the flow remains laminar as pressure decreases; losses are overestimated considerably at Pa (10^{-5} torr).

Based on the results shown in table 7, it is reasonable to assume that the parasitic windage losses are negligible at pressure of 0.0013 Pa (10^{-5} torr). This magnitude of pressure is easily obtained with conventional pumpdown equipment, and maintaining it in a completely sealed enclosure will not be difficult.

Table 7
Total Windage Losses for 7-kW h Rotor Described in Table 4

Pressure	P (laminar)	P (molecular flow)
Pa (torr)	(watts)	(watts)
0.13 (10^{-3})	193	225
0.013 (10^{-4})	61	31
0.0013 (10^{-5})	21	3

Suspension System

The purpose of the suspension system is to provide stable support for the ring rotor in both the axial and radial directions with the minimum amount of power loss (that is, minimum parasitic loss) and longest possible mechanical life.

Based upon these requirements, a modified electromagnetic system was chosen. A cross section schematic of one of the two suspension coils, previously shown in figure 4, is shown in figure 5. The principle of operation of this system is to establish a steady-state magnetic flux in the air gap (by the samarium-cobalt permanent magnets) and allow the change in magnetic reluctance, due to axial sag, to support the rotor weight without active axial control. The exact amount of axial sag can be reduced to any desired value by simply increasing the number of teeth on the moving iron. If the radial gap clearance is sensed, then the radial rotor position can be actively controlled by varying the current through the stationary force coil, thus holding the radial gap clearance constant. (At least one direction must be active for the system to be stable.)

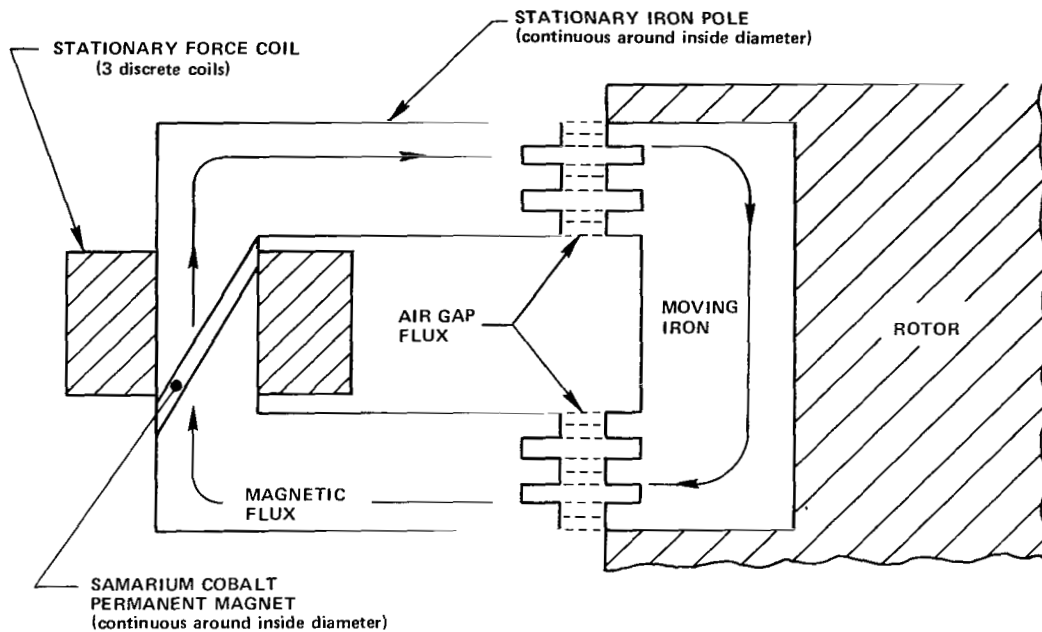


Figure 5. Cross section of magnetic suspension.

Shown in appendix F are the detailed design equations for the 10-kW h rotor described in table 6. These results are summarized in the following list.

Rotor Suspension Characteristics

Axial	Radial
Passive, Minimum Reluctance	Servoed
Max. Load = 222 kg (488 lb)	Nominal Flux Density = 0.615 tesla (40kl/in ²)
Rotor (ID) = 1.8 m (70.8 in.)	Control Flux Density = ± 0.154 tesla (± 10 kl/in ²)
Clearance = 0.152 cm (0.06 in.) radial	Peak Force = 1110 kg (2440 lb)
No. of Teeth = 16	Control Sensitivity = 3.36 kg/W (7.4 lb/W)
Tooth Width = 0.157 cm (0.062 in.)	21 Segments
Stiffness = 6930 kg/cm (8000 lb/in.)	

The type of electromagnetic forcer described in this report has been successfully applied to a 223-N (50-lbf) ring rotor intended for angular momentum control in spacecraft applications* (reference 17). It is anticipated that the radial gap sensors and the force coil electronics (to provide the current for the stationary force coils) will be directly applicable to the spokeless ring storage system described in this report.

It is further anticipated that the parasitic wattage losses of the suspension system will be small. Eddy current losses, due to the movement of magnetic field, will be eliminated by making the stationary force coil continuous around the inner circumference of the ring. Hysteresis losses, due to the cycling of a magnetic field in the iron, will be dependent on the amount of mechanical tolerance in the shape of the ring and the perturbing forces which act on the storage system. Because it is doubtful that either of these factors will be large, the hysteresis losses are considered negligible. The only other loss is the quiescent power dissipation of the control circuit for the force coil. Based on a spacecraft momentum control device, it is felt these losses can be made quite small (a few watts).

An additional advantage of this magnetic suspension system is that there will be little penalty in hysteresis losses if it is necessary to use a stronger iron alloy for the moving iron. The fact that a stronger alloy can be used provides a firmer basis for the previous assumption of treating the storage ring as a single element of composite material (no iron considered).

Motor/Generator

The purpose of the motor/generator is to provide for the input and output of electrical energy from the moving rotor. The general requirements for the motor/generator system are:

- Be compatible with the spokeless magnetically levitated ring geometry,
- Provide long life and high energy conversion efficiencies,
- Have negligible parasitic losses,
- Be functional as both a motor or generator, and
- Have a constant voltage output as the rotor speed changes (generator).

Several types of motor/generator concepts were considered for the spokeless ring flywheel system. These are:

- Annular momentum control device type (reference 17),
- Ironless armature*,

*Fisher, R.L., "Ironless Armature Torque Motor," Contract NAS5-11481, Sperry Marine Systems Division, Charlottesville, Virginia, 1968.

- Variable strength field (having both stationary armature and field windings),
- Homopolar d.c. motor.

None of these were satisfactory by themselves, and the final design is a combination of the best features of the above systems and the results of a number of Goddard Space Flight Center programs dating back to the mid 1960s.

The cross section configuration of the ring rotor motor/generator is shown in figure 6. This geometry results in a variable field homopolar d.c. motor (with stationary armature and field windings) and will provide a constant voltage variable frequency output from a rotor whose speed changes by a factor of 2 (from ω_{\max} to $\omega_{\max}/2$). The stationary armature and field magnet is continuous around the inside circumference of the ring rotor. The motor/generator field is established by two permanent magnet rings (which provide the magnetic bias flux) and is then modulated by field coils on the two legs of the stationary magnetic field circuit. The stationary armature winding projects into the air gap slot of the rotor moving field. Note that the rotor-moving field poles are all north on the upper rings and south on the lower. (There are a finite number of equally spaced pole projections on both the upper and lower moving iron pole rings.) This configuration (homopolar) means that the flux does not alternate in direction from pole to pole; rather, salient poles form regions of high flux density, and the current return path is in a region of low flux density rather than reversed polarity.

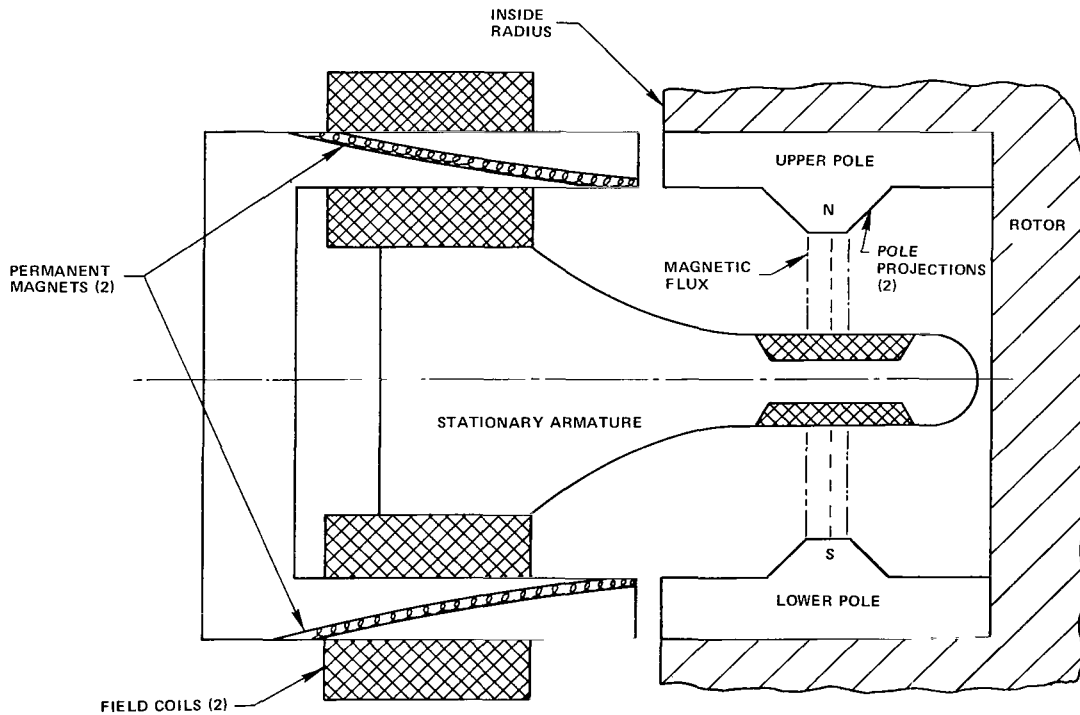


Figure 6. Motor/generator system.

The field flux included in the motor/generator rotor poles may be utilized as part of the magnetic suspension system (see previous section). However, for the sake of simplicity in this report, the functions of these systems are considered separately.

To achieve the proper phase output from the motor/generator the armature windings will be electronically switched (commutated) thus providing the most efficient electrical-to-mechanical energy conversion and allowing complete symmetry in both motor and generator modes. Shown in appendix G are the detailed design equations for the motor/generator of the 10-kW h rotor described in table 6. The results of these calculations are summarized in the list below.

Homopolar PM d.c. Motor/Generator Characteristics

Peak Power	= 10 kW
Diameter	= 1.8 m (72 in.)
No. Poles	= 84 (0.81 × 2.28 cm (0.36 × 0.9 in.))
Flux Density	= 0.3 ± 0.1 tesla (19.5 ± 6.5 kl/in. ²)
Armature Resistance	= 0.087 ohms, R

160 turns/phase

30 parallel paths

28 A.W.G.

Inductance = 3 μ henry

Pole Freq. = 11,424/s maximum

- Field Current = 0
 - $K_v = 0.201 \text{ V/rad/s}$
 - $K_t = 1.07 \text{ kg m/A (0.148 lb ft/A)}$
 - $E_a = 129\text{V@ } 102 \text{ RPS (75\%)}$
- Field Current = +3.5 A
 - $K_v = 0.269 \text{ V/rad/s}$
 - $K_t = 1.44 \text{ kg m/A (0.200 lb ft/A)}$
 - $E_a = 115\text{V@ } 68 \text{ RPS (50\%)}$
- Field Current = -3.5 A
 - $K_v = 0.152 \text{ V/rad/s}$

$$K_t = 0.81 \text{ kg m/A (0.112 lb ft/A)}$$

$$E_a = 130\text{V@ 136 rps}$$

- Armature Current = 90 A maximum rated

$$I_a^2 R = 705 \text{ W @ peak load}$$

- Constant voltage, charge/discharge

50% to 100% speed

1 hr charge to 7 kW h

IR Drop = 7.8 V at maximum rated current

Efficiency, at peak load = 93% $I_f = 0$

$$= 89.5\% I_f = 3.5$$

At $\frac{1}{2} \omega$ max speed

$$I_f^2 R \text{ losses} = 420 \text{ W}$$

The electronic commutation function has been successfully applied to a 223-N (50-lbf) annular momentum control device (AMCD) ring rotor (reference 17) and the sensors and commutating circuitry will be applicable in this design. The output of the motor/generator (see figure 3) will be rectified and inverted to 60 Hz, 110 V a.c. power by conventional means, and no difficulty is expected in this area.

It is anticipated that the parasitic wattage losses for the motor/generator system will be low. The motor/generator is of essentially "ironless" construction meaning that the rotating field gap flux does not pass through any stationary magnetic iron; thus, there are no magnetic losses due to hysteresis or eddy currents in the armature. Under no-power conditions, the only losses are due to eddy currents of the armature wires which reside in the field gap. However, these losses may be minimized by reducing the physical size of the wires in the gap by means of parallel paths. Since the rotor will change speed over a long period of time (typically twice a day), the hysteresis losses of the iron is negligible. The other hysteresis losses (the same as those in the magnetic suspension) are due to the mechanical tolerance in the shape of the ring and perturbing forces which may cause periodic variations in the moving iron ring into and out of the magnetic flux. Since it is doubtful that either of these factors will be large, the hysteresis losses are considered negligible. The only other parasitic loss is the power dissipation in the field coils. Because the majority of field flux is provided by the permanent magnets, this loss can be kept very low (less than 5 percent of the total stored energy in the system).

When power is being drawn from the system, there is an additional $I_a^2 R$ loss in the wires of the armature. Worst-case calculations have shown that this loss can be easily held to a maximum of 5 percent of the total stored energy in the system.

Efficiency for the charge and discharge cycles is expected to be about 80 percent, and the coast (storage) cycle efficiency is expected to be about 90 percent.

CONCLUSIONS

There is a demonstrated need for energy storage systems for peak shaving in the electric power industry. Energy storage in rotating flywheels provides one solution provided that the system life is greater than 20 years, and high energy conversion efficiencies (greater than 60 percent) can be achieved.

One of the most important measures of performance of flywheel energy storage is energy density (stored energy per unit of rotor weight). The highest energy densities (and, in a general sense, the lowest capital cost of stored energy per dollar) of flywheel rotors are obtainable using composite materials in uniaxially stressed geometries. A thin spokeless composite ring rotor (ID/OD = 0.9) has a larger energy density than a circular brush superflywheel and nearly as large (92 percent) as the theoretical maximum for a thin-ring geometry. Thus a thin-ring spokeless geometry is extremely favorable for the rotor of an energy storage system.

It has been suggested in this report that attention must be given to all the modules of a complete energy storage system if long life and high efficiency are to be achieved. In particular a general storage system consists of storage, environment, suspension, and input/output modules.

To best utilize the thin-ring, spokeless geometry as the storage module, a permanent magnetic flux, biased, magnetic levitation system has been configured. This system provides for active control in the radial direction with passive magnetic constraints in the axial direction. Based on the proposed configuration, little derating of the flywheel energy density is expected, and parasitic losses have been shown to be negligible.

The spokeless ring is also used as the moving element of a specially developed variable field homopolar d.c. motor/generator. All parasitic losses are shown to be small, and the system functions equally well as either a motor or a generator.

Design formulas for the parasitic windage loss of the spokeless ring flywheel have been developed. Because operation at reduced pressures is a requirement in minimizing windage losses, it has been shown that it is better to consider the fluid (air) as a molecular stream rather than a simple laminar flowing fluid.

While this report addresses the application for electric power industry use, it is clear that this technology is also compatible with solar- and wind-powered systems. In addition, the storage concept is also useful for emergency standby use for hospitals, elevators, computers, and other emergency type applications where power interruptions would cause hazards or hardships.

SUGGESTIONS FOR FUTURE WORK

If a prototype of the spokeless, magnetically levitated ring is to produce near-theoretical energy densities, some additional theoretical work must be done. In particular, the ring element, composed of both composite material and magnetically soft iron, must be optimized for mechanical strength, practical fabrication feasibility, and minimum reluctance. The following suggestions are offered:

- The ring design, to be modeled by a NASTRAN finite element program, should take into account the anisotropic properties of the composite material and the presence of iron in the ring. Various configurations can be investigated theoretically and the one with the highest energy density selected.
- Dynamic analysis of the mechanical/structural system, electrodynamics, and, in particular, cross coupling effects should be undertaken. This would include coupling of in-plane and out-of-plane rim modes due to radial and axial suspension inputs.
- A cost analysis should be performed on the complete storage system. The best way to do this is to take the ring geometry obtained in the first section and develop a general computer program which takes into account the total costs of all system components. This program should include both projected fabrication and material costs and should be capable of determining the best system size for a given total energy storage requirement.

After completion of the analysis, design, build, and test a total mechanical capacitor (7 kW h) system.

Goddard Space Flight Center
National Aeronautics and Space Administration
Greenbelt, Maryland November 1975

REFERENCES

1. Kalhammer, F.R., and P.S. Zygielbaum, "Potential for Large-Scale Energy Storage in Electric Utility Systems," A.S.M.E. Paper 74-WA/ENER-9, November 1974.
2. Keller, W.E., "Energy Storage for the Electric Power Industry," *Conference on Advanced Energy Systems*, Denver, Colorado, June 20, 1974.
3. Laaspere, T., and A.O. Converse, "Creative Electric Load Management," *IEEE Spectrum*, February 1975, pp. 46-50.
4. Laaspere, T., "Energy Storage I, II," *Science*, **184**, 1974, pp. 785-787 and pp. 884-887.
5. Clerk, R.C., "The Utilization of Flywheel Energy," *Transactions S.A.E.*, **72**, 1964, pp. 508-543.
6. Rabenhorst, D.W., "Primary Energy Storage and the Superflywheel," Applied Physics Laboratory/Johns Hopkins University, TG-1081, September 1969.
7. Rabenhorst, D.W., "New Concepts in Mechanical Energy Storage," *Intersociety Energy Conversion Engineering Conference*, Las Vegas, Nevada, 1970, pp. 2-95 to 2-99.
8. Rabenhorst, D.W., "Potential Applications for the Superflywheel," *Intersociety Energy Conversion Engineering Conference*, Boston, Massachusetts, 1971, pp. 1118-1125.
9. Rabenhorst, D.W., "The Application of Wood Technology to Kinetic Energy Storage," *APL Technical Digest*, **2**, (5), (Applied Physics Laboratory, The Johns Hopkins University), 1972, pp. 2-12.
10. Rabenhorst, D.W., "Superflywheel Energy Storage System," *Wind Energy Conversion System Workshop*, ed., Savino, J.M., Washington, D.C., NASA TM X-69786, 1973, pp. 137-145.
11. Rabenhorst, D.W., "The Multirim Superflywheel," Applied Physics Laboratory, Johns Hopkins University, TG-1240, August 1974.
12. Rabenhorst, D.W., "Metals and Composites in Superflywheel Energy Storage Systems," *SAMPE Quarterly*, **6**, 1975, pp. 23-28.
13. Rabenhorst, D.W., and R.J. Taylor, "Design Considerations for a 100-Megajoule/500-Megawatt Superflywheel," Applied Physics Laboratory, Johns Hopkins University, TG-1229, December 1973.
14. Post, R.F., and S.F. Post, "Flywheels," *Scientific American*, **229**, (6), 1973, pp. 17-23.

15. Dugger, G.L., A. Brandt, J.F. George, and L.L. Perini, "Flywheel and Flywheel/Heat Engine Hybrid Propulsion Systems for Low-Emission Vehicles," *Intersociety Energy Conversion Engineering Conference*, Boston, Massachusetts, 1971, pp. 1126-1141.
16. Dugger, G.L., A. Brandt, J.F. George, L.L. Perini, D.W. Rabenhorst, R.R. Small, and R.O. Weiss, "Heat-Engine/Mechanical-Energy-Storage Hybrid Propulsion Systems For Vehicles," Applied Physics Laboratory, Johns Hopkins University, Final Report CP-011, 1972.
17. Anderson, W.W., and N.J. Groom, "The Annular Momentum Control Device (AMCD) and Potential Applications," Langley Research Center, NASA TN D-7866, March 1975.
18. Studer, P.A., "Magnetic Bearing," U.S. Patent 3,865,442, February 11, 1975.
19. Studer, P.A., "Magnetic Bearings for Spacecraft," Goddard Space Flight Center, TM X-66111, January 1972.
20. Studer, P.A., "Electric Motive Machine Including Magnetic Bearing," U.S. Patent 3,694,041, September 26, 1972.
21. Lawson, L.J., "Design and Testing of High Energy Density Flywheels for Application to Flywheel/Heat Engine Hybrid Vehicle Drivers," *Intersociety Energy Conversion Engineering Conference*, Boston, Massachusetts, 1971, pp. 1142-1150.
22. Wang, C.T., *Applied Elasticity*, McGraw-Hill Book Co., New York, 1953.
23. Notti, J.E., A. Cormack III, and W.C. Schmill, "Integrated Power/Attitude Control System (IPACS) Study, Volume I - Feasibility Studies," NASA CR-2383, 1974.
24. Notti, J.E., A. Cormack III, W.C. Schmill, and W.J. Klein, "Integrated Power/Attitude Control System (IPACS) Study, Volume II - Conceptual Designs," NASA CR-2384, 1974.
25. Keckler, C.R., and Jacobs, K.C., "A Spacecraft Integrated Power/Attitude Control System," *Intersociety Energy Conversion Engineering Conference*, San Francisco, California, 1974.
26. Studer, P.A., "Development of a Sealed Brushless D.C. Motor," NASA TN D-2819, May 1965.
27. Casaday, W.M., "Reaction Wheel with Brushless D.C. Motor Drive," NASA CR-388, April 1966.
28. "Breakthrough in Magnetic Materials," *Solid State Power Conversion*, March/April 1975, pp. 56-57.
29. Morgenthaler, G.F., and S.P. Bonk, "Composite Flywheel Stress Analysis and Materials Study," *SAMPE Science of Advanced Materials and Process Engineering*, 12, Article D-5, Anaheim, California, 1967.
30. Rohsenow, W., and H. Choi, *Heat, Mass, and Momentum Transfer*, Prentice-Hall, New Jersey, 1961, p. 290.

APPENDIX A

SUMMARY OF UNIT CONVERSIONS

<u>Given</u>	<u>Multiply By</u>	<u>To Obtain</u>
Specific energy in (N m)/N	1	Specific energy in J/N
Specific energy in in. lbf/lbf	3.139×10^{-5}	Specific energy in Wh/lbf
Specific energy in in. lbf/lbf	2.54×10^{-2}	Specific energy in J/N
Specific energy in in. lbf/lbf	6.921×10^{-5}	Specific energy in Wh/kgf
Specific energy in kWh/lbf	8.09×10^5	Specific energy in J/N
Specific energy in kWh/lbf	2205	Specific energy in Wh/kgf
Specific energy in Wh/kgf	367	Specific energy in J/N
Specific energy in Wh/lbf	809	Specific energy in J/N
Specific energy in Wh/N	9.81	Specific energy in Wh/kgf
Kinetic energy in in. lbf	0.113	Kinetic energy in J
Momentum in ft lbf s	1.36	Momentum in J s
Mass moment in ft lbf s ²	1.36	Mass moment in J s ²

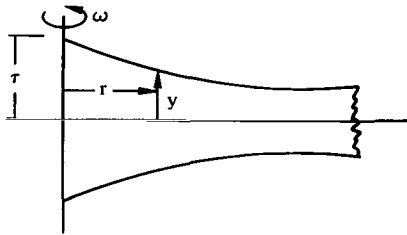


APPENDIX B

EVALUATION OF VARIOUS ROTOR SHAPES

CONSTANT STRESS DISK (Reference 22)

Geometrical Configuration



$$y = \tau e^{-\frac{\rho \omega^2 r^2}{2\sigma}}$$

$$\text{ID} = 0 \text{ solid}$$

$$\text{OD} = \infty$$

Formulas

$$\text{K.E.} = \frac{2\pi \tau \sigma^2}{\rho \omega^2}$$

$$E_w = 1.000 \frac{\sigma}{\gamma}$$

$$\sigma_{\max} = \sigma_r = \sigma_\theta = \sigma \text{ constant}$$

$$E_w = K_s \times \frac{\sigma}{\gamma}$$

$$K_s = 1.000$$

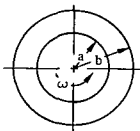
$$E_{vs} = 1.000 \sigma$$

$$\frac{W}{V} = \frac{E_v}{E_w} = 1.000 \gamma$$

PIERCED DISK (Reference 22)

Geometrical Configuration

Both radial and circumferential stresses are considered.



a = inner radius

b = outer radius

τ = thickness - constant

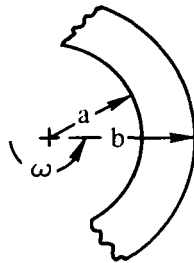
Formulas

$$\begin{aligned}
 \text{K.E.} &= \frac{1}{4} \rho \omega^2 \tau \pi \{b^4 - a^4\} \\
 E_w &= \frac{1}{4} \frac{\rho \omega^2}{\gamma} \times \{b^2 + a^2\} \\
 \sigma_{\max} &= \frac{(3 + \nu)}{4} \left(1 + \left(\frac{a}{b}\right)^2 \frac{1 - \nu}{3 + \nu}\right) \rho \omega^2 b^2 \\
 E_w &= K_s \times \frac{\sigma}{\gamma} \\
 K_s &= \frac{\left(\frac{a}{b}\right)^2 + 1}{3 + \nu + \left(\frac{a}{b}\right)^2 (1 - \nu)} \\
 E_{vs} &= K_s \sigma \times \left(1 - \left(\frac{a}{b}\right)^2\right) \\
 \frac{W}{V_s} &= \frac{E_{vs}}{E_w} = \gamma \times \left(1 - \left(\frac{a}{b}\right)^2\right)
 \end{aligned}$$

HOOP

Geometrical Configuration

A thin pierced disk where it is assumed $\sigma_r = 0$ and $\sigma_\theta = \rho \omega^2 b^2$ (i.e., a/b approaches 1.0).



a = inner radius
 b = outer radius
 τ = thickness - constant
 σ_r = radial stress = 0
 σ_θ = tangential stress

Formulas

$$\begin{aligned}
 \text{K.E.} &= \frac{1}{4} \rho \omega^2 \tau \pi \{b^4 - a^4\} \\
 E_w &= \frac{1}{4} \frac{\rho \omega^2}{\gamma} \times \{b^2 + a^2\} \\
 \sigma_{\max} &= \rho \omega^2 b^2
 \end{aligned}$$

$$E_w = K_s \times \frac{\sigma}{\gamma}$$

$$K_s = \frac{1 + \left(\frac{a}{b}\right)^2}{4}$$

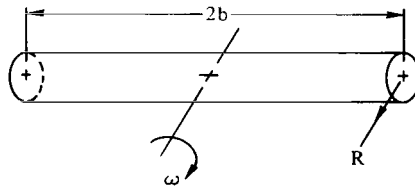
$$E_{vs} = K_s \times \sigma \times \left(1 - \left(\frac{a}{b}\right)^2\right)$$

$$\frac{W}{V_s} = \gamma \times \left(1 - \left(\frac{a}{b}\right)^2\right)$$

NOTE: A given volume could be occupied by a number of independent hoops with the effect of the overall a/b being much less than 1. For this case, the hoop formulas apply. (This was the analysis used by Rabenhorst (reference 11).)

SINGLE FILAMENT-ROUND

Geometrical Configuration



2b = length of rod
R = radius of rod
Vol = volume of rod

Formulas

$$K.E. = \frac{1}{2} \times \rho \omega^2 \times \frac{1}{12} \{3R^2 + 4b^2\} \times Vol$$

$$E_w = \frac{1}{24} \frac{\rho \omega^2}{\gamma} \times \{3R^2 + 4b^2\}$$

$$\sigma_{\max} (@ r = 0) = \frac{1}{2} \rho \omega^2 b^2$$

$$E_w = K_s \times \frac{\sigma}{\gamma}$$

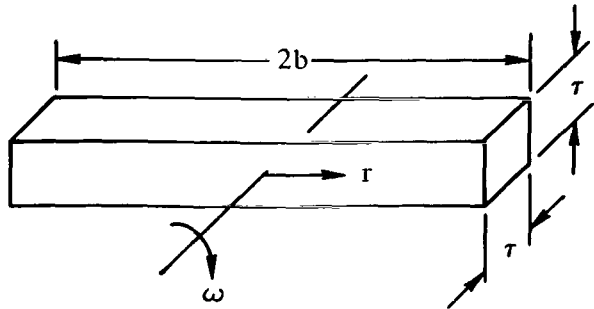
$$K_s = \frac{1}{3} + \frac{1}{4} \left(\frac{R}{b}\right)^2$$

$$E_v = \frac{K_s}{b} \times R \times \sigma = K_s \times \sigma \times \left\{\frac{R}{b}\right\}$$

$$\frac{W}{V_s} = \frac{E_{vs}}{E_w} = \gamma \times \left(\frac{R}{b}\right)$$

SINGLE FILAMENT—SQUARE

Geometrical Configuration



$2b$ = length of rod

τ = thickness of side

Vol = volume of rod

Formulas

$$K.E. = \frac{1}{2} \times \rho \omega^2 \times \frac{1}{12} \{ \tau^2 + 4b^2 \} \times \text{Vol}$$

$$E_w = \frac{1}{24} \frac{\rho \omega^2}{\gamma} \{ \tau^2 + 4b^2 \}$$

$$\sigma_{\max} (@v=0) = \frac{1}{2} \rho \omega^2 b^2$$

$$E_w = K_s \times \frac{\sigma}{\gamma}$$

$$K_s = \frac{1}{3} + \frac{1}{12} \left(\frac{\tau}{b} \right)^2$$

$$E_{vs} = K_s \times \sigma \times \left\{ \frac{2\tau}{\pi b} \right\}$$

$$\frac{W}{V_s} = \frac{E_v}{E_w} = \gamma \times \left\{ \frac{2\tau}{\pi b} \right\}$$

BRUSH—n SINGLE FILAMENTS

Geometrical Configuration

It is assumed that n-square or round rods are rotating about a common axis. (See Rabenhorst, reference 8 or 13).

Formulas

$$K.E. = n \times (\text{K.E. of 1 square or round rod})$$

$$E_w = \text{same as for 1 square or round rod}$$

$$\sigma_{\max} (@ r = 0) = \text{same as for 1 square or round rod}$$

$$E_w = K_s \times \frac{\sigma}{\gamma}$$

$$K_s = \text{same as for 1 square or round rod}$$

$$E_{vs} = n \times (E_v \text{ for 1 square or round rod})$$

$$\frac{W}{V_s} = \frac{E_v}{E_w} = n \times \left(\frac{W}{V_s} \text{ for 1 square or round rod} \right)$$

NOTE: Rabenhorst (reference 13) used a total of 20 square rods each 1.27 cm (0.5 in.) on a side and 2.25 m (88 in.) total length (2b) for this case:

$$n = 20$$

$$K_s = 1/3$$

and the percent of the swept volume occupied by rods is approximately 15 percent.



APPENDIX C

ID/OD RATIO TO ELIMINATE RADIAL DELAMINATION DUE TO CENTRIFUGAL STRESSES

PROBLEM

Given a pierced disk where:

a = inner radius

b = outer radius

locate the radius ratio (a/b) where the following condition holds;

$$\sigma_{r(\max)} \leq 0.005 \sigma_{\max}$$

SOLUTION

Assume the formulas for an isotropic pierced disk apply (reference 22)

$$\sigma_r = \left(\frac{3 + \nu}{8} \right) \rho \omega^2 b^2 \left\{ 1 + (a/b)^2 - \frac{(a/b)^2}{(\nu/b)^2} - \left(\frac{r}{b} \right)^2 \right\}$$

$$\sigma_\theta = \left(\frac{3 + \nu}{8} \right) \rho \omega^2 b^2 \left\{ 1 + (a/b)^2 + \frac{(a/b)^2}{(\nu/b)^2} - \left(\frac{1 + 3\nu}{3 + \nu} \right) (r/b)^2 \right\}$$

Where:	ρ	= mass density	<u>Unit</u> kg/m ³
	ν	= Poisson ratio of contraction in the radial direction due to extension in the circumferential direction, 0.33 assumed.	
	ω	= angular velocity	rad/s
	σ_r	= radial stress	Pa
	σ_θ	= circumferential stress	Pa

For convenience, the nondimensional radial and tangential stress are shown plotted versus radius ratio (for various a/b ratios) on figure C-1.

The maximum stress occurs at the inner radius and is given by:

$$(\sigma_{\theta})_{\max} = \sigma_{\theta m} = \left(\frac{3+\nu}{4}\right) \rho\omega^2 b^2 \left(1 + \frac{1-\nu}{3+\nu} (a/b)^2\right) \quad (C-1)$$

$$(\sigma_r)_{\max} = \sigma_{rm} = \left(\frac{3+\nu}{8}\right) \rho\omega^2 b^2 (1 - (a/b))^2 \quad (C-2)$$

Dividing equation C-1 by C-2 and applying the constraint given in the problem statement:

$$\frac{\sigma_{rm}}{\sigma_{\theta m}} = \frac{(1 - a/b)^2}{2 \left\{1 + (a/b)^2 \frac{1-\nu}{3+\nu}\right\}} = 0.005$$

which can be solved to obtain:

$$a/b \cong 0.9$$

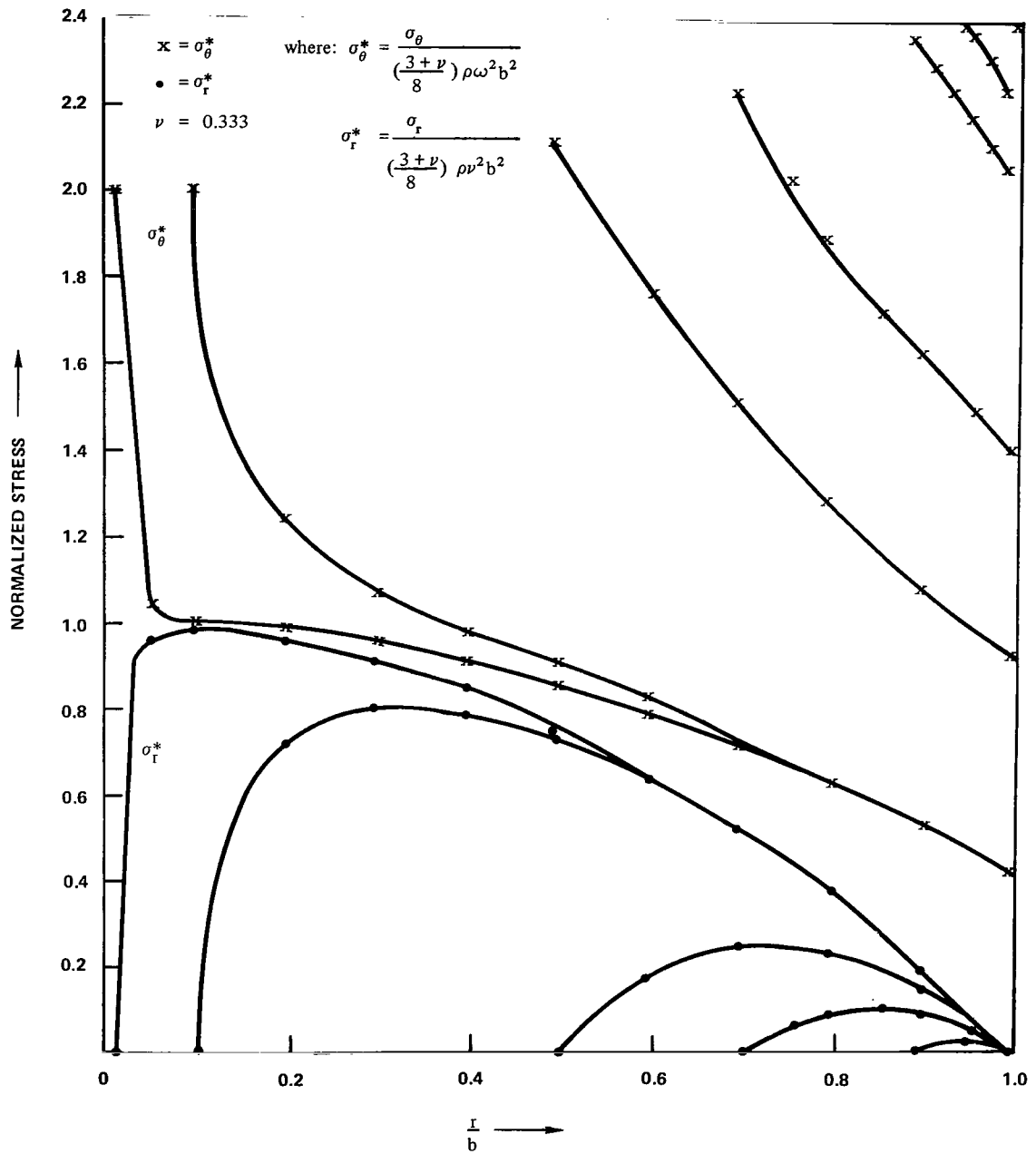


Figure C-1. Normalized stress versus radius ratio.



APPENDIX D

SIMPLIFIED DESIGN EQUATIONS FOR SIZING A STORAGE ROTOR

PROCEDURE

The procedure outlined below is applicable to sizing a composite energy storage ring. It is assumed that the entire rotating weight is made of Kevlar-49 composite material, and there is no derating necessary because of the iron (magnetic flux path elements) which is carried on the inside radius of the ring. First

- Decide on the amount of energy which is to be stored (TE = total stored energy) in units of joules (kW h), and
- Determine the required weight (W) of the ring.

$$E_w = K_s \times \frac{g}{\gamma}$$

where: K_s = shape factor = 0.46 for a thin ring of $a/b = 0.9$

$$\frac{g}{\gamma} = 0.717 \cdot 10^5 \text{ J/N (89 W h/lbf)}$$

for Kevlar-49 composite being used at 59 percent of its ultimate tensile strength.

$$E_w = 3.30 \cdot 10^4 \text{ J/N (40.9 W h/lbf)}$$

$$W = \frac{TE \text{ (joules)}}{3.30 \times 10^4} \text{ (N in newtons)}$$

$$W = \frac{TE(Wh)}{40.9} \text{ (W in lbf)}$$

Determine the size of the ring.

$$W = \gamma \tau \pi (b^2 - a^2)$$

$$= \gamma \tau \pi b^2 (1 - (a/b)^2)$$

$$= 0.597 \gamma \tau b^2$$

(D-1)

(Recall a/b is fixed at 0.9 by radial delaminating stress limits.)

Choose a reasonable b and solve equation D-1 for τ at this point.

b = known (designer's choice)

τ = known (from equation D-3 since weight - W - is known)

$a = 0.9b = \text{known}$

Determine the speed of rotation by solving equation C-1 for ω (assume 0.33 for ν).

$$\omega = \sqrt{\frac{4 \sigma_{\theta m}}{\rho (3 + \nu) b^2 (1 + [0.81]) \frac{1 - \nu}{3 + \nu}}} \quad (\text{D-2})$$

$$\omega = \frac{1.02}{b} \sqrt{\frac{\sigma_{\theta m} g}{\gamma}} \quad \text{rad/s} \quad (\text{D-3})$$

If the storage ring is made of Kevlar-49 (see reference 13) operating at 59 percent (this represents a safe fatigue limit) of the ultimate tensile strength, then:

$$\sigma_{\theta m} = 0.973 \text{ G Pa (141,000 psi)}$$

$$\gamma = 13.6 \text{ k N/m}^3 \text{ (0.05 lbf/in.}^3\text{)}$$

$$g = 9.80 \text{ m/s}^2 \text{ (386 in./s}^2\text{)}$$

and equation D-3 becomes:

$$\omega = \frac{854}{b} \quad \text{rad/s if } b \text{ in meters}$$

or

$$\omega = \frac{3.37 \times 10^4}{b} \quad \text{rad/s if } b \text{ in inches}$$

$$\text{RPM} = \frac{\omega}{2\pi} \times 60 \quad \text{rot/min}$$

Finally, check to see $(\sigma_r)_{\max}$ and $(\sigma_{\theta})_{\max}$ are all within design specifications.

EXAMPLE

Store a total energy of 36 MJ (10 kWh).

1. $TE = 36 \text{ MJ (10 kWh)}$

2. $W = \frac{36 \times 10^6}{3.3 \times 10^4} = 1091 \text{ N} \left(\frac{10^4}{40.9} = 244 \text{ lbf} \right)$

$$3. \quad 1091 = 0.597 \gamma \tau b^2$$

$$\gamma = 13.6 \text{ kN/m}^3 \text{ (0.05 lbf/in.}^3\text{)}$$

Assume: $b = 1 \text{ m (39.37 in.)}$

$$a = 0.9 \text{ m (35.43 in.)}$$

$$\tau = \frac{1091}{0.597 (136 \times 10^3) \rho} = 0.134 \text{ m (13.4 cm (5.27 in.))}$$

$$4. \quad \omega = \frac{854}{b} = \frac{854}{1} = 854 \text{ rad/s}$$

$$= \frac{(845) \times 60}{2\pi} = 8163 \text{ rpm}$$

Check the maximum stresses for these conditions using equations (C-1) and (C-2).

$$(\sigma_r)_{\max} \text{ at } r = ab = 0.95 \text{ m (37.35 in.)}$$

$$(\sigma_r)_{\max} = \left(\frac{3.33}{8} \right) \left(\frac{13.6 \times 10^3}{9.80} \right) (855)^2 (1)^2 (1 - (0.9))^2$$

$$= 4.22 \times 10^6 \text{ Pa (612 psi)}$$

$$(\sigma_\theta)_{\max} \text{ at } r = a = 0.9 \text{ m (35.43 in.)}$$

$$(\sigma_\theta)_{\max} = \left(\frac{3.33}{4} \right) \left(\frac{13.6 \times 10^3}{9.80} \right) (855)^2 (1^2 + 0.2 (0.9)^2)$$

$$= 9.81 \times 10^8 \text{ Pa (141,000 psi)}$$

and

$$\frac{(\sigma_r)_{\max}}{(\sigma_\theta)_{\max}} = 4.3 \times 10^{-3} = 0.43 \text{ percent}$$

which is well within the strength limits of Kevlar-49.



APPENDIX E

WINDAGE LOSSES FOR A RING FLYWHEEL

WINDAGE LOSSES OF A SPINNING RING

The following symbols have been used in the deviation which follows:

<u>Symbol</u>	<u>Name</u>	<u>SI Unit</u>	<u>English Units</u>
ρ	Fluid mass density	kg/m ³	lbf s ² /in. ⁴
ω	Angular velocity	rad/s	rad/s
b	Outer ring radius	m	inches
a	Inner ring radius	m	inches
τ	Ring thickness	m	inches
P_r	Air pressure	Pa	torr
P	Power loss	W	W hp
μ	Absolute viscosity	Pa s	lbf s/in. ²
C_D	Drag coefficient	-	-
R_e	Reynolds number	-	-
	$\frac{\omega r^2 \rho}{\mu}$	-	-
M	Mach number	-	-
	V tip/V sound		

The drag on a spinning ring (containing no spokes) is skin friction drag which occurs on the inside and outside diametral surfaces and on the top and bottom ring faces. If it is assumed, for a worst case condition, that the ring is rotating in still air, then the calculation for the total drag on the body proceeds as shown.

NOTE: This procedure must be used (especially at pressures less than 0.13 N/m² (10⁻³ torr)) since the gas looks more like a molecular stream than a fluid.

1. Calculate the R_e for both the OD and ID of the ring. Use:

$$R_e = \frac{\omega r^2 \rho}{\mu}$$

$\mu = 2.58 \times 10^{-9}$ (lbf s/in.²) or 1.78×10^{-5} (Pa s) for air. This is independent of pressure.

$$\rho = \frac{P_r}{760} 1.15 \times 10^{-7} \text{ (lbf s}^2\text{/in.}^4\text{)} \text{ or } (P_r/1.013 \times 10^5) \times (1.23) \text{ kg/m}^3$$

ω = angular velocity (rad/s)

r = radius (inches) or (m)

2. Calculate the Mach number for both the OD and ID of the ring.

$$M = \frac{V_{\text{TIP}}}{V_{\text{sound}}}$$

$$V_{\text{sound}} = 335 \text{ m/s (1100 ft/s) at room temperature}$$

3. Calculate the Z_1 nondimensional parameter for both OD and ID

$$Z_1 = \frac{\sqrt{R_e}}{1.5M}$$

4. Use Z_1 to compute a drag coefficient for both the outside and inside diameters by using the following formula (reference 30):

$$C_D = \frac{1.33}{Z_1^2 M} \left[(\text{EXP}(Z_1^2)) \text{ERFC } Z_1 - 1 + \frac{2Z_1}{\sqrt{\pi}} \right] \quad (\text{E-1})$$

(or the graph shown on page 290 of reference 30) subject to the following conditions.

- (a) for $Z_1 < 1.0$ you are in the free molecular flow region

$$C_D = \frac{0.674}{M}$$

- (b) For $1 < Z_1 < 10$ use the graph or formula to obtain C_D

- (c) For $Z_1 > 10$ look at the R_e number on the OD. If $R_e < 10^4$ use the laminar flow equations for drag. If the $R_e < 10^5$, use the turbulent flow equations. If $10^4 < R_e < 10^5$ average the power losses computed using both the laminar and turbulent equations. These losses will be generally much larger than those computed in (a) and (b).

5. Compute the power losses according to the formulas shown below. These were derived by considering the drag coefficient to:

- Be a constant for $Z_1 < 10$

- Be equal to (reference 30, page 78) — $C_D = \frac{1.328}{\sqrt{R_e}}$ for $Z_1 > 10$ and $R_e < 10^4$

- Be equal to (reference 30): $C_D = \frac{0.072}{\sqrt{R_e^{0.2}}}$ $Z_1 > 10$ $10^5 < R_e < 10^6$

EQUATION

Region

$$Z_1 < 10 \quad P \text{ (watts)} = C_D \rho \omega^3 1.24 (b^5 - a^5) + 3.14 \tau (b^4 + a^4)$$

$$Z_1 > 10 \quad R_e < 10^4 \quad P \text{ (watts)} = \rho^{0.5} \omega^{2.5} (8.82 \times 10^{-3}) (b^4 - a^4) + (1.76 \times 10^{-2}) \dot{\tau} (b^3 + a^3)$$

$$Z_1 > 10 \quad R_e > 10^5 \quad P \text{ (watts)} = \rho^{0.8} \omega^{2.8} (1.10 \times 10^{-2}) (b^{4.6} - a^{4.6}) + (2.99 \times 10^{-2}) \dot{\tau} (b^{3.6} + a^{3.6})$$

where the following units must be used:

ρ	fluid mass density	kg/m ³
ω	angular velocity	rad/s
b	outside radius	m
a	inside radius	m

Region

$$Z_1 < 10 \quad P \text{ (watts)} = C_D \rho \omega^3 0.14 (b^5 - a^5) + 0.355 \dot{\tau} (b^4 + a^4)$$

$$Z_1 > 10 \quad R_e < 10^4 \quad P \text{ (watts)} = \rho^{0.5} \omega^{2.5} (1.20 \times 10^{-5}) (b^4 - a^4) + (2.39 \times 10^{-5}) \tau (b^3 + a^3)$$

$$Z_1 > 10 \quad R_e > 10^5 \quad P \text{ (watts)} = \rho^{0.8} \omega^{2.8} (2.13 \times 10^{-4}) (b^{4.6} - a^{4.6}) + (5.76 \times 10^{-4}) \dot{\tau} (b^{3.6} + a^{3.6})$$

where the following units must be used:

ρ	fluid mass density	lbf s ² /in. ⁴
ω	angular velocity	rad/s
b	outside radius	in.
a	inside radius	in.



APPENDIX F

FLYWHEEL—SUSPENSION

To suspend a 111-kg (244-lb) flywheel at its inside diameter magnetically with a passive axial (vertical), active radial system:

Rotor weight = 111 kg (244 lb)

Assume design for 2g (gravity) capability

Load = 222 kg (488 lb)

Rotor inner circumference = 1.8 m 70.8 in.

$$\frac{\times 3.14}{5.65 \text{ m}} \qquad \frac{\times 3.14}{222 \text{ in.}}$$

Force must be produced tangentially at the rotor/stator interface.

$$\frac{2170.7 \text{ N}}{5.65 \text{ m}} = 384.2 \text{ N/m}$$

The radial force across this interface is required to be about ten times this force.*

$$F_R = 21707 \text{ newtons}$$

Assuming a nominal gap flux density of 0.62 tesla.

$$F = \frac{\beta^2 A}{k}$$

$$k = 2.5 \times 10^{-6}$$

$$\beta = \text{teslas}$$

$$A = \text{m}^2$$

$$A = k \frac{F}{\beta^2} = k \frac{21707}{0.3844} = 0.1422 \text{ m}^2$$

$$A = \frac{0.1422 \text{ m}^2}{(\text{Circumference}) = 5.65 \text{ m}} = 0.0252 \text{ m}$$

$$\text{Supplied by motor field:} = \frac{0.0061 \text{ m}}{0.0191 \text{ m}}$$

*See Mechanical Technology Inc., Report 75 TR 21, January 1975.

For symmetry, this will be divided into two elements each with two active surfaces. The face width of each will be 0.476 cm, further subdivided into teeth of 0.159 cm width to reduce the sag at 1g to 25 to 50 percent of that dimension.

The overall axial stiffness should be:

$$\frac{1085 \text{ N}}{0.076 \text{ cm}} = 14,244 \text{ N/cm}$$

The length of magnet required will be:

$$\begin{aligned} NI &= \frac{\beta \times 2 \times \ell_g}{0.000126} \\ &= \frac{0.62 \times 2 \times 0.1524}{0.000126} \\ &= 1500 \text{ AT} \end{aligned}$$

Using Sm Co₅ magnet at H = 3200 AT/cm:

$$\ell_m = 0.469 \text{ cm}$$

At this operating point, the magnet can supply 0.4 tesla. Since the required flux across the gap is 0.62 tesla at a total width of 2.52 cm and allowing for leakage:

$$w_m = \frac{0.62 \times 0.478 \times 1.8}{0.4} = 1.33 \text{ cm}$$

Since the force is proportional to the square of the flux density, a two-to-one change in force can be achieved by a ± 25 percent modulation of the magnet ampere turns. The effective air gap, for the control winding, includes the permanent magnet; therefore, the coil ampere turns required:

$$\frac{1}{4} \left(1 + \frac{0.469}{1.33} \times \frac{0.305}{0.468} \right) 1500 \text{ AT} = 462 \text{ AT}$$

To modulate the assembly, a group of four pole spans will be considered. The core cross section will be 36.12 cm² (5.6 in.²) if wound around the magnet. Assuming a path length of 30.5 cm (12 in.) per conductor and maximum of 40 W per coil, 360 turns of No. 27 A.W.G. wire would result in a peak coil current of 1.3 A and a coil resistance of 18.5 ohms. A 0.65-cm² (0.1-in.²) coil cross section would be required.

APPENDIX G

MOTOR/GENERATOR CALCULATIONS

Schematics are shown in figures G-1 through G-4.

Type: Electronically Commutated Ironless Armature d.c. Variable Field, Induced Flux Homopolar.

Power	Input/Output	10,000 W
Diameter	Nominal	1.8 m
Speed		641 ±214 rad/s
Voltage	Nominal	120 V
Current	Max	90 A
No. of Poles		84
No. of Phases		3
No. of Conductors Per Phase		136
No. of Parallel Paths		30
Wire Size		28 A.W.G.
Resistance	delta	0.087 ohms
	per phase	0.13 ohms
	per path	3.9 ohms
Flux Density	Pole Gap	0.3 tesla (19.5 kl/in. ²)
	Interpole	0.15 tesla (9.75 kl/in. ²)
Pole Area		0.0002 m ² (0.324 in. ²)
Pole Span		0.068 m (2.7 in.)

$$E = N \frac{d\theta}{dt} \times 10^{-8} \text{ V}$$

$$N = 160 \text{ conductors}$$

$$\Delta\theta/\text{cm} = 1.38 \text{ kilolines/cm } (\Delta\theta/\text{in.} = 3.5 \text{ kl/in.})$$

$$\omega = 102 \text{ rps (75\% speed)}$$

$$E_a = 129 \text{ V}$$

$\text{Force} = \beta I \ell = \text{Newtons}$ $\Delta\beta = 0.15 \text{ tesla}$ $I = 2.9 \text{ A}$ $\ell = 0.0091 \text{ m}$ $= 0.0036 \text{ N/conductor}$ $\quad \underline{\times 160 \text{ conductor}}$ 0.63336 N $\quad \underline{\times 30 \text{ paths}}$ 19.0 N $\quad \underline{\times 0.914 \text{ m}}$ 17.37 N m $\quad \underline{\times 102 \text{ rps}}$ 11200 W	$= 8.8 \times 10^{-5} \text{ lb}$ 9.75 kl/in.^2 2.9 A 0.36 in. $= 0.00895 \text{ lb/conductor}$ $\quad \underline{\times 160 \text{ conductor}}$ 0.1433 lb $\quad \underline{\times 30 \text{ paths}}$ 4.3 lb $\quad \underline{\times 3 \text{ ft}}$ 12.9 lb ft $\quad \underline{\times 102 \text{ rps}}$ 11217 W
--	---

$$I_{\max} = 87 \text{ A} \quad I^2 R = 659 \text{ W}$$

Inductance, from previous design:

$$L = 0.00041 \times \left(\frac{160}{1872} \right)^2 = 3 \times 10^{-6} \text{ henry}$$

$$L/R = \frac{3 \times 10^{-6}}{0.087} = 34.4 \mu\text{s}$$

$$\text{Frequency, } \omega_{\max} = 136 \text{ rps} \times 84 \text{ poles} = 11,424 \text{ Hz}$$

$$\text{Pole face size} = 0.92 \times 2.29 \text{ cm} \quad (0.36 \times 90 \text{ in.})$$

$$\text{Conductor turn length} = 2 (2.29 \text{ cm} + 3.43 \text{ cm}) \quad (2(0.9 \text{ in.} + 1.35 \text{ in.}))$$

$$\begin{array}{r}
 11.44 \text{ cm/conductor} \\
 \times 2 \text{ conductor/pole} \\
 \hline
 22.88 \\
 \times 80 \text{ poles (active)} \\
 \hline
 1830 \text{ cm}
 \end{array}$$

$$\begin{array}{r}
 4.5 \text{ in./conductor} \\
 \times 2 \text{ conductor/pole} \\
 \hline
 9.0 \\
 \times 80 \text{ poles (active)} \\
 \hline
 12 \times 720 \text{ in.} \\
 \hline
 60 \text{ ft}
 \end{array}$$

$$\times 0.00214 \text{ ohms/cm (\#28 A.W.G.)} \quad \times 0.0653 \text{ ohms/ft (\#28 A.W.G.)}$$

$$\begin{array}{r}
 30 \times \begin{array}{l} 3.92 \text{ ohms/path} \\ 0.1309 \text{ ohms/phase} \\ \times 0.67 \\ \hline 0.087 \text{ ohms (Delta)} \end{array}
 \end{array}$$

$$\begin{array}{r}
 30 \times \begin{array}{l} 3.918 \text{ ohms/path} \\ 0.1306 \text{ ohms/phase} \\ \times 0.67 \\ \hline 0.087 \text{ ohms (Delta)} \end{array}
 \end{array}$$

Total conductor length =

$$\begin{array}{r}
 1646 \text{ m} \\
 \times 0.00745 \text{ kg/m} \\
 \hline
 12.3 \text{ kg}
 \end{array}
 \quad = 60 \times 3 \times 30 = 5400 \text{ ft}$$

$$\begin{array}{r}
 \times 0.0005 \text{ lb/ft} \\
 \hline
 2.7 \text{ lb}
 \end{array}$$

$$\begin{array}{r}
 \text{Motor-only rotor iron} = 645 \text{ cm}^3 \\
 5.27 \text{ kg}
 \end{array}$$

$$\begin{array}{r}
 39.4 \text{ in.}^3 \\
 11.6 \text{ lb}
 \end{array}$$

FIELD—PERMANENT MAGNET

Flux per pole	= 6.3 kilolines	@ 0.2 tesla	(@ 19.5 kl/in. ²)
Interpole leakage	= 6.3 kilolines	@ 0.15 tesla	(@ 9.75 kl/in. ²)
Pole gap	= 0.635 cm	(0.25 in.)	
Stator gap	= 0.1524 cm	(0.06 in.)	

$$HF = \frac{\beta \ell g}{3.192} \text{ ampere turns}$$

$$= 2452 \text{ AT}$$

$$= 0.95 \text{ cm (0.375 in.) Samarium Cobalt}$$

FIELD—CONTROL COIL

$$\text{Control flux density} = 0.1 \text{ tesla } (\pm 6.5 \text{ kl/in.}^2)$$

$$HF = \frac{2919}{3} = 973 \text{ AT}$$

$$\theta = 16.64 \text{ kl/4 poles}$$

$$@\beta = 1.89 \text{ tesla (122 kl/in.}^2)$$

$$\text{Area} = 0.88 \text{ cm}^2 \text{ (0.136 in.}^2)$$

diameter = 1.05 cm (0.416 in.)

21 coils, I_f = 0.17 A/coil

$\frac{974 \text{ AT}}{0.17 \text{ A}}$ = 5800 turns

Wire size, 36 A.W.G.

Coil resistance, 700 ohms

Max dissipation 20 W/coil
 $\frac{21}{420 \text{ watts, field}}$

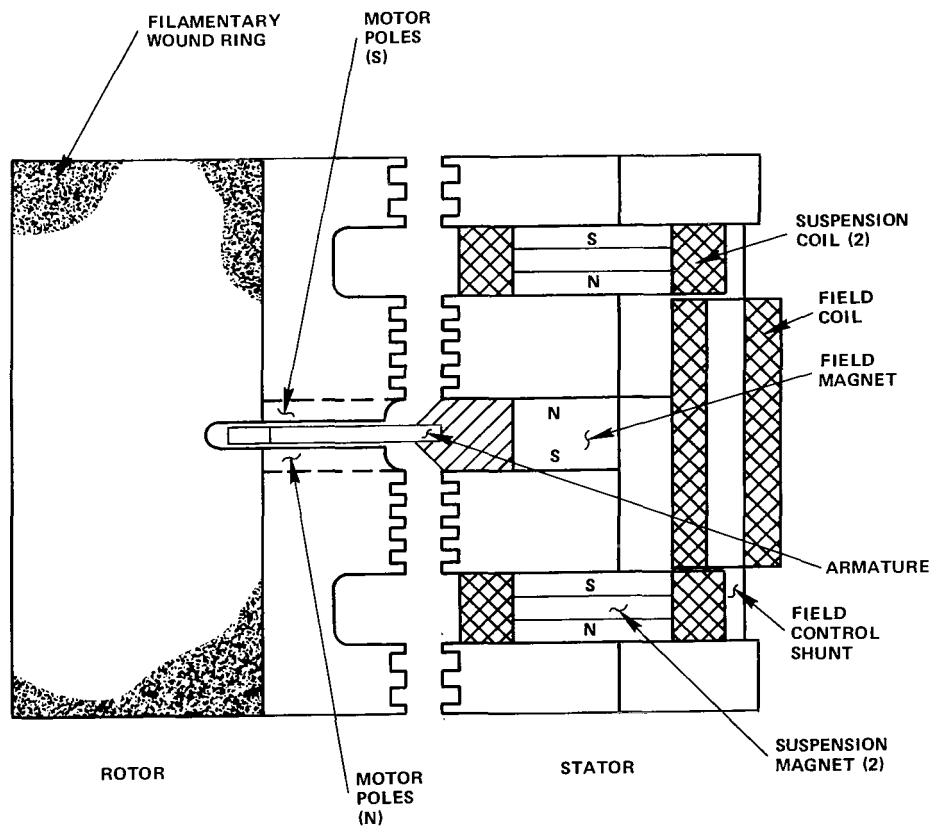


Figure G-1. Rotor/stator cross section.

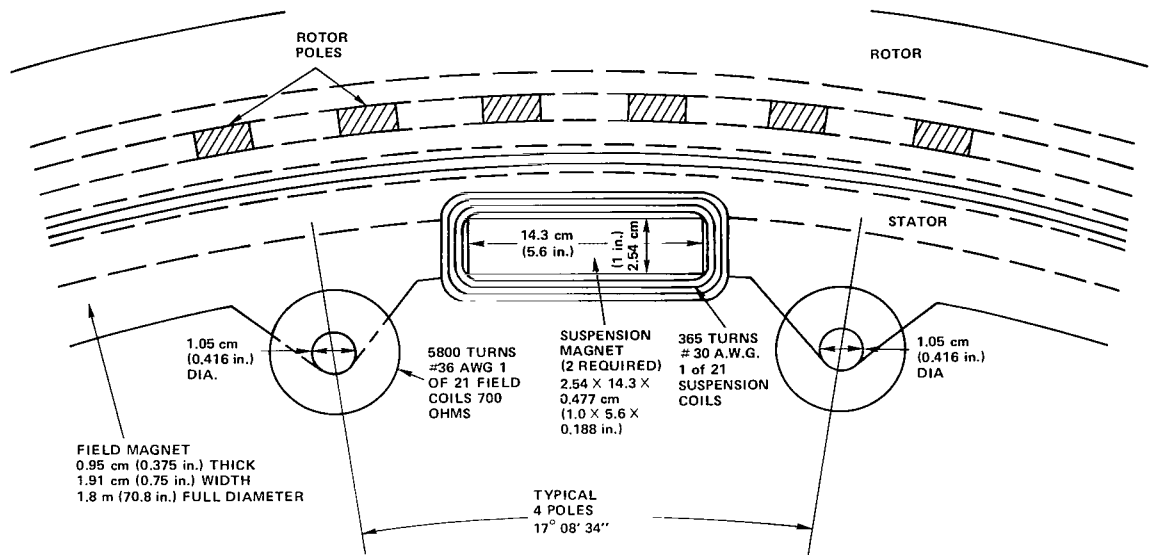


Figure G-2. Rotor/stator top view.

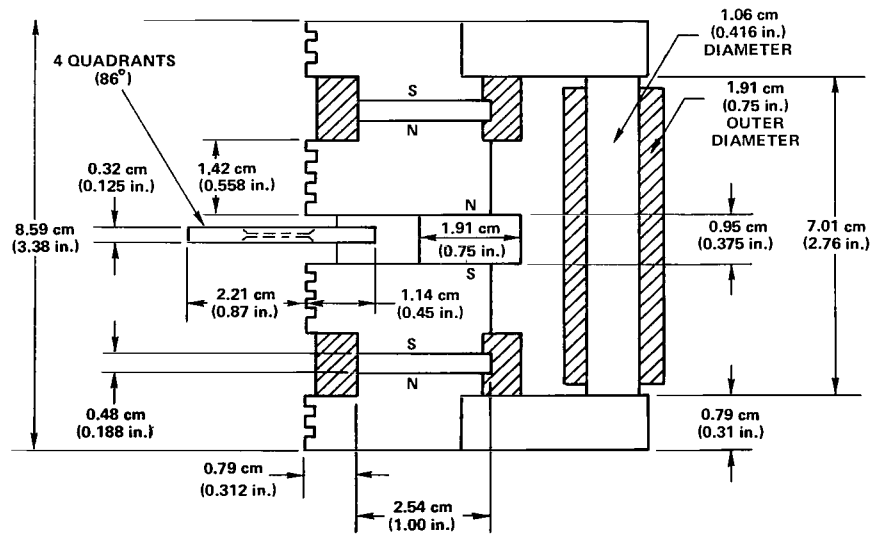


Figure G-3. Stator/motor suspension.

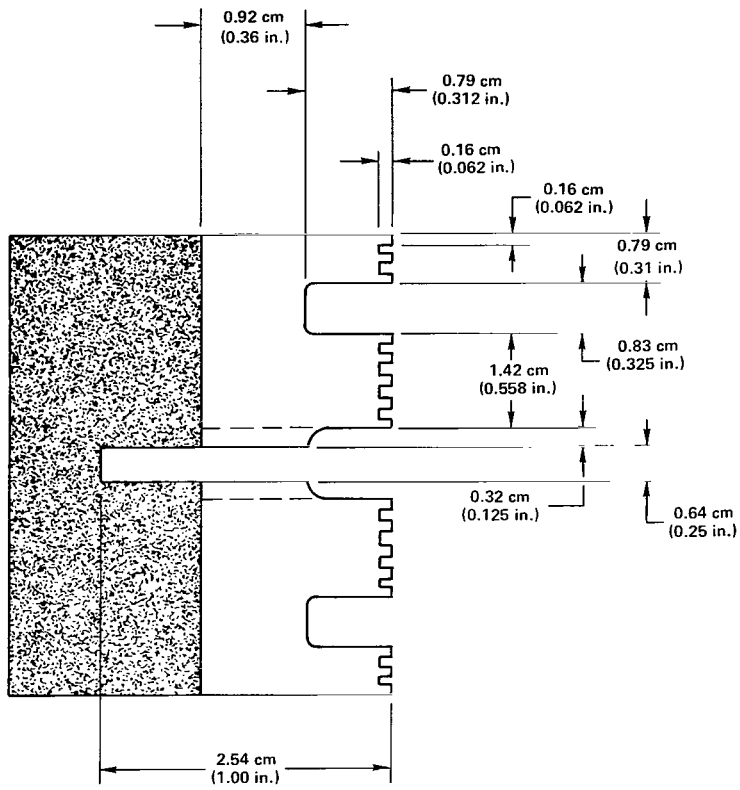


Figure G-4. Rotor.



382 001 C1 U E 760312 S00903DS
DEPT OF THE AIR FORCE
AF WEAPONS LABORATORY
ATTN: TECHNICAL LIBRARY (SUL)
KIRTLAND AFB NM 87117

POSTMASTER: If Undeliverable (Section 158
Postal Manual) Do Not Return

"The aeronautical and space activities of the United States shall be conducted so as to contribute . . . to the expansion of human knowledge of phenomena in the atmosphere and space. The Administration shall provide for the widest practicable and appropriate dissemination of information concerning its activities and the results thereof."

—NATIONAL AERONAUTICS AND SPACE ACT OF 1958

NASA SCIENTIFIC AND TECHNICAL PUBLICATIONS

TECHNICAL REPORTS: Scientific and technical information considered important, complete, and a lasting contribution to existing knowledge.

TECHNICAL NOTES: Information less broad in scope but nevertheless of importance as a contribution to existing knowledge.

TECHNICAL MEMORANDUMS: Information receiving limited distribution because of preliminary data, security classification, or other reasons. Also includes conference proceedings with either limited or unlimited distribution.

CONTRACTOR REPORTS: Scientific and technical information generated under a NASA contract or grant and considered an important contribution to existing knowledge.

TECHNICAL TRANSLATIONS: Information published in a foreign language considered to merit NASA distribution in English.

SPECIAL PUBLICATIONS: Information derived from or of value to NASA activities. Publications include final reports of major projects, monographs, data compilations, handbooks, sourcebooks, and special bibliographies.

TECHNOLOGY UTILIZATION PUBLICATIONS: Information on technology used by NASA that may be of particular interest in commercial and other non-aerospace applications. Publications include Tech Briefs, Technology Utilization Reports and Technology Surveys.

Details on the availability of these publications may be obtained from:

SCIENTIFIC AND TECHNICAL INFORMATION OFFICE

NATIONAL AERONAUTICS AND SPACE ADMINISTRATION
Washington, D.C. 20546